LAPPEENRANTA UNIVERSITY OF TECHNOLOGY
LUT School of Engineering Science
Degree program in Technical Physics

Anna-Maria Baronenkova

CHARACTERIZATION AND TESTING OF NOVEL SINGLE CORE PHOSPHATE FIBERS

Examiner: Professor, D.Sc. Erkki Lähderanta
Supervisor: Associate Professor Laeticia Petit

Dedicated to the memory of my grandfathers, Eugene and Anatolii, who valued education and science above all

ABSTRACT

Lappeenranta University of Technology
LUT School of Engineering Science
Degree program in Technical Physics

Anna-Maria Baronenkova

Characterization and testing of novel single core phosphate fibers

Master's thesis
2019

60 pages, 48 figures

Examiners: Professor, D.Sc. Erkki Lähderanta

Associate professor Laeticia Petit

Keywords: optical fiber, photonics, erbium, ytterbium.

This work is devoted to the study of novel optical fibers doped with Er^{3+} ions. Fibers were drawn from the phosphate glasses with different compositions. One of the optical fibers was drawn from a heat-treated preform in order to grow Ag nanoparticles while another fiber was drawn from $NaYF_4$: Er^{3+}, Yb^{3+} nanoparticles containing glass preform. Before discussing the changes in the shape of the emission band at 1.5 μm when in contact with N-Methylaniline, the analysis of the composition and of the structure of the fibers are presented.

ACKNOWLEDGEMENTS

I would like to thank my supervisor Professor Erkki Lähderanta for giving me the great opportunity to study as a Double Degree student in Lappeenranta University of Technology. He supported all of us during the study process and helped us when we had problems.

This work has been carried out in the Photonics Laboratory at Tampere University. Thus, I want to thank my supervisor – Associate Professor Laeticia Petit for her patience, invaluable instructions and support. In addition, I would like to acknowledge Dr. Regina Gumenyuk for her help and important advices and Dr. Turkka Salminen for conducting the SEM and EDS analysis.

Finally, I would like to thank my family and close friends (Gleb, Milena, Yuliya, Tatyana, Eugenia, Kseniya and Daria) for their encouraging words and support during my studies and writing this diploma. Especially I want to mention the contribution of my parents Aleksandr and Elena – your support is priceless and means a lot for me.

Tampere, April 2019

Anna-Maria Baronenkova

LIST OF ABBREVIATIONS AND SYMBOLS

ΔT	difference between onset of crystallization and glass transition temperatures
θ_c	critical angle
$\rho(\nu)$	radiation density
τ_f	lifetime of the fluorescence
τ_R	radiative lifetime
A_{rad}	radiative process
B_{12}	constant of proportionality
E_1	energy on the first laser state
E_2	energy on the second laser state
G	ground state
$h\nu_{12}$	energy between 1 and 2 states
N_1	population on the first laser state
N_2	population on the second laser state
T_g	glass transition temperature
T_m	melting temperature
T_p	crystallization temperature (peak temperature)
T_x	onset of crystallization temperature
W_{nr}	non-radiative process
ATR	attenuated total reflectance
BSE	backscattered electrons
CVD	chemical vapor deposition
CW	continuous wave
DC	downconversion
DFB	distributed feedback laser
DTA	differential thermal analysis
DSC	differential scanning calorimetry
EDFA	erbium doped fiber amplifier
EDS	elemental dispersive X-ray spectroscopy

ESA	excited state absorption
ETU	energy transfer upconversion
FEWS	fiber evanescent wave spectroscopy
FTIR	Fourier-transform infrared spectroscopy
HT	heat treatment
IR	infrared
LED	light emitting diode
MCT	mercury cadmium telluride
MCVD	modified chemical vapor deposition
MMF	multimode fiber
NIR	near-infrared
NMA	N-Methylaniline
NPs	nanoparticles
OVD	outside vapor deposition
OSA	optical spectrum analyzer
PA	photon avalanche
RE	rare earth
REF	reference
SE	secondary electrons
SEM	scanning electron microscope
SMF	single-mode fiber
TIR	total internal reflection
UC	upconversion
UV	ultraviolet
VPAD	vapor-phase axial deposition

CONTENTS

1. INTRODUCTION

Photonics deals with the physical theory of the generation of light, its detection, transformation, emission, transmission, signal processing and amplification. [Qu, 06] [Ye, 12]. Most applications of photonics are involved in the field of visible and IR radiation, although scope of application of photonics extends to the entire wide region of the spectrum.

As a global generalized direction, photonics combines several different sciences such as: laser physics, optoelectronics, fiber and integrated optics, nonlinear optics, optical communications and optical signal processing, just to cite a few.

Like optics, photonics describes phenomena associated with the properties of the light. This is a broad discipline, the methods of which can be used both in the medicine and in the electrical engineering. However, all applications are based on the detection and manipulation of photons.

After the invention of the first laser in 1960, laser diode was discovered in 1970's as well as the optical fiber for data transmission and the first optical fiber amplifier that was doped with erbium. All these achievements formed the basis for the creation of telecommunication in the late 20th century and helped to create the Internet infrastructure.

Research on novel doped active fibers is the main topic of this master thesis.

The thesis consists of 5 chapters, Chapter 6 listing all the references used in this thesis. Chapter 2 presents some background about photonics, laser glasses and optical fibers. Chapter 3 consists of the experimental data: it is explained how the samples were fabricated and characterized. The experimental results and discussion are presented in Chapter 4. Conclusion is given in Chapter 5.

2. BACKGROUND

Nowadays, photonics has a huge number of scientific and technological applications, including the production of lasers, medical diagnostics and therapy, biological sensing, information display techniques and optical computing [Ye, 12]. Specialists in the field of photonics (and sciences involved in it) have developed laser technologies to treat tumors and carry out other operations, and have also worked on the creation of "light Wi-Fi". In addition, based on the scientific experience associated with the study of the nature of light and its interaction with various materials, new materials with unique properties have been of great interest.

Microphotonics and nanophotonics areas include photonic crystal devices and solid-state devices. Nanoparticles and metal nanoparticles can be great example of objects with size-dependent optical properties [Pr, 04]. Photonic integrated systems are optical active integrated semiconductor photonic devices consisting of at least two different functional units (amplification regions and lattice-based laser mirrors).

Photonics is also engaged in the study of photonic devices for use in optical communications. That area of research focuses on the introduction of photonic devices, such as high-speed photon networks, and the scope of the research on optical regenerators that improve the quality of optical signals.

2.1 Glasses for photonics

With investigating of high power fiber lasers, researchers have reduced cost of the lasers, power consumption and increased their reliability. Schematic installation of such laser is presented in the fig. 1.

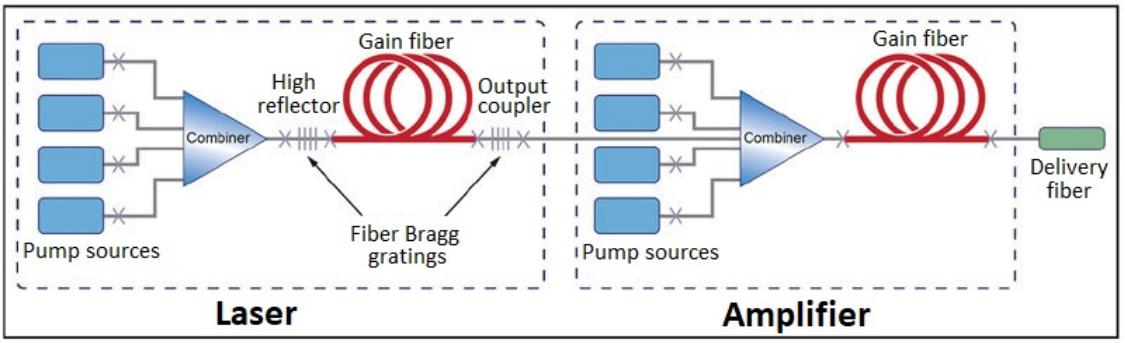

Figure 1. Schematic diagram with main components of the high power fiber laser system [Tb, 17].

The fiber gain medium of laser is usually rare earth doped fiber, shown with red color on the scheme. The fiber with grey color is passive to transmit light and the splices on the figure are denoted “X”. Pump sources are usually diode lasers and they could be in two variations: single emitters where each semiconductor chip includes one emitter and diode bars with multiple emitters on one semiconductor.

2.1.1 Definition of the glass

Glass is material that has a glass transition temperature at which it solidifies into an amorphous solid; amorphous means that glass does not have a long range order or periodic atomic arrangement. Thus, glass is a non-crystalline solid material, which has atomic arrangement similar to that of the liquid.

As presented in fig. 2, when a liquid substance is cooled down from high temperature, its molecular motion slows down. When the temperature reached the crystallization temperature (T_x), the substance crystallize (solid black curve in fig. 2).

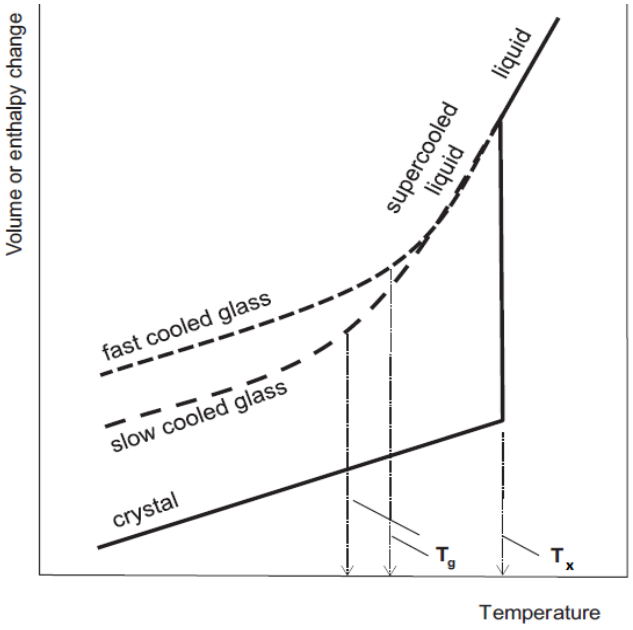

Figure 2. Temperature dependence of a specific volume and enthalpy [Ya, 00].

When the temperature continues to decrease, the substance becomes a supercooled liquid. When its temperature decreases below the glass transition temperature (T_g) this substance becomes a solid amorphous material also known as glass.

In other word, after melting, the glass material in liquid form needs to be rapidly cooled to avoid the formation of crystals.

2.1.2 Types of the glasses

There are different types of glasses depending on their components used in the composition:

Silica glass: this glass is made from silica. ^{29}Si (silica isotope; it is stable, spin is ½; widely used in the spectroscopy) is the most abundant element in the earth's crust and silica has received one of the greatest amount of attention due to its ubiquity in solid state materials (silicates, zeolites, glasses). This glass is resistant to high temperature (up to 1000 °C) and thermal shock, it transmits visible and ultraviolet radiation. Because of its high optical transparency, silica glass has been widely studied as a host material [Ba, 06] [Bu, 09]. Production of that glass is associated with high energy costs, since silica glass is a

refractory raw material and is difficult to melt. Silica glass has tetrahedral units in its structure, where silicon is located in the center and it is surrounded by oxygen as shown in fig. 3.

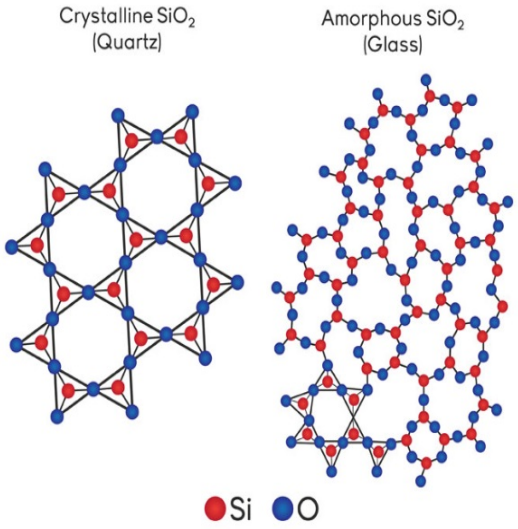

Figure 3. Crystalline and amorphous atomic structure of the silicate based glasses [Nd].

Silicate based glasses: most important glasses are the sodium borosilicate glasses with Na_2O-B_2O_3-SiO_2 glass system [Vo, 94]. The addition of boron oxide to the composition of the material increases its resistance to thermal shock up to 5 times, improving also the chemical properties of the glass. A large-scale example of usage is a mirror created on the basis of borosilicate glass for the world's largest telescope. Because of the high chemical resistance, borosilicate glass is used for manufacture of pipes and laboratory and chemical glassware, products for domestic use [Vo, 94]. For example, DURAN® products from the borosilicate glass show high resistance to water, neutral and acid solutions, alkaline solutions and organic substances [Th].

Sodium silicate glasses are made of two components: sand and soda. Usually, furnace temperature region lays between about 1000 and 1400 °C. A large number of manufacturers prefer sodium silicate as an adhesive because it has a low cost and is not toxic. In addition, sodium silicate is one of the materials, which is used in production of the silica gel. The main disadvantage is that such type of glass is soluble in water.

Lead glasses: lead oxide is usually added in glasses to improve their dielectric properties. Lead glasses are used as the best insulating compound in television tubes, oscilloscopes, capacitors and so on [Sh, 05]. The presence of the lead in the glass gives the material an additional shine and sparkle, which is often used in the manufacture of artistic products, dishes etc. [Vo, 94]. Lead glasses are now used as a protection screens from the X-ray in medical field, laboratory research, on nuclear power stations and in atomic applications. This shielding screen (fig. 4) has a high transparency allowing one to take a look inside the chamber at no risk.

Figure 4. X-ray shielding lead glass [Le].

Phosphate glasses: such type of glasses are technically very important as a high power laser host. Their refractive indexes remain constant even under high power electromagnetic field. Rare earth ions are well isolated from each other in the vitreous network preventing self-quenching effect. Therefore, phosphate glasses are good for optical communications, lasers and amplifiers [Hu, 01] [Ji, 00] [Kn, 03]. However, phosphate fibers have higher phonon energy than silica glasses, which is disadvantageous for the upconversion emission [Mi, 13] [Sh, 07a]. Schematic content of the Q^i phosphate networks is presented in fig. 5. Index “i” denotes the number of bridging oxygens for each PO_4 unit in the network.

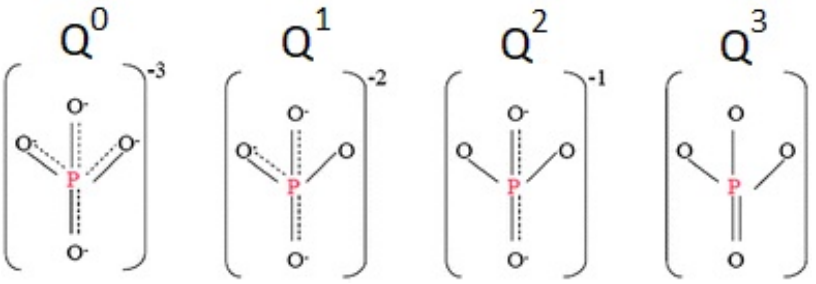

Figure 5. Schematic image of tetrahedral PO_4 units in the phosphate glass [Yu, 13].

Only ultraphosphate Q^3 tetrahedral system has double bonded oxygens in it; Q^2, Q^1 and Q^0 have non-bridging oxygens [Br, 00a] [Br, 00b].

2.1.3 Laser glasses

Lasers are the coherence sources of the monochromatic radiation with high intensity in UV, visible and IR ranges. Fig. 6 shows three types of laser systems. Two energy levels have populations N_1 and N_2, and energies E_1 and E_2.

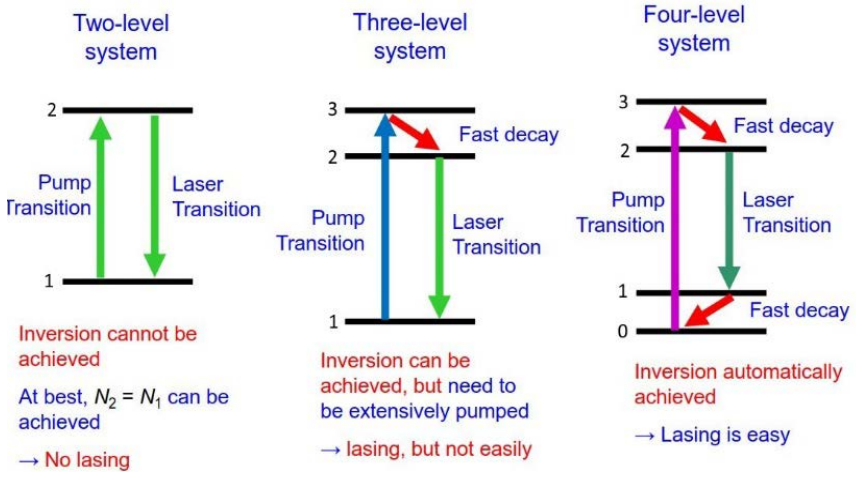

Figure 6. Different energy diagrams of pumping and laser transition: for lasers three energy levels needed [Ka, 99].

Energy between these levels is presented in equation 1.

$$h\nu_{12} = E_2 - E_1 \quad (1)$$

The atoms can be transferred from first level to second level by absorbing the energy. After that, population N_1 at lower level will be reduced at rate which is proportional both to the radiation density $\rho(\nu)$ and to the population at first level as shown in equation 2, where B_{12} is just a constant of proportionality:

$$\frac{dN_1}{dt} = -B_{12}\rho(\nu)N_1 \quad (2)$$

The product $B_{12} * \rho(\nu)$ is the transition rate from first level to second, per atom and per unit frequency. After atom is pumped to the upper energy state, it will return to lower energy state and emit some amount of light.

There are two possible ways: radiative decay with emission of photon or non-radiative decay when excitation energy is converted into vibrational quanta of the surroundings [Ya, 00].

Fluorescence lifetime τ_f at excited second energy state E_2 is given by the combination of probabilities for radiative (A_{rad}) and non-radiative processes (W_{nr}) (see equation 3):

$$\frac{1}{\tau_f} = A_{rad} + W_{nr} = \frac{1}{\tau_R} + W_{nr} \quad (3)$$

where τ_R is a radiative lifetime. The fluorescence lifetime varies from picoseconds to hundreds of nanoseconds range. A variety of non-radiative and radiative processes usually occurs following the absorption of light on route to the observation of molecular luminescence [Om, 99].

Laser glasses contain rare earth elements from the lanthanide group of the Periodic System (fig. 7).

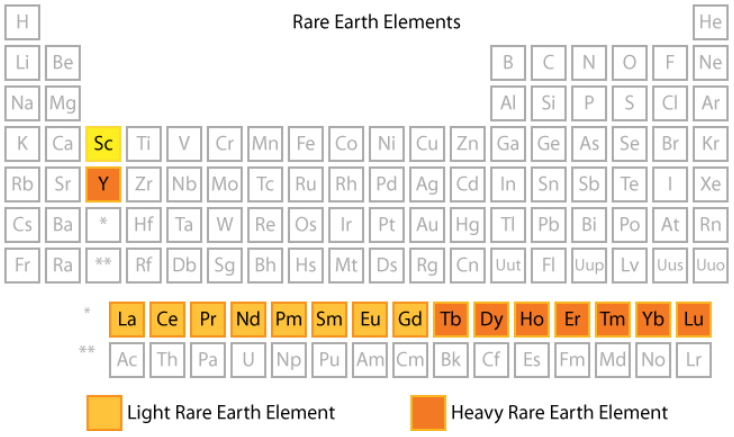

Figure 7. Periodic table showing the rare earth elements [Se, 16].

Lanthanides are ideal for converting radiation in the UV and IR ranges due to presence of plenty energy states. RE nanoparticles gives ability to luminesce from visible to IR range

[Pe, 17b]. The most common elements used for lasers are erbium, neodymium and ytterbium. One of the first solid-state lasers was demonstrated in 1961 with the glass doped by Nd^{3+} ions. Lasing in the Nd^{3+}-doped multi-component glass fiber was published only three years later.

Nowadays researchers and developers are interested in the optic lasers and amplifiers, which are based on erbium-doped glasses. The interest for erbium-doped glasses arose with shift of the main operational range for optical fiber communications to the 1.5 μm. Erbium was found and extracted in 1843 from mineral, which is called gadolinite near the Swedish city of Ytterby [En, 06]. Erbium is indicated by the symbol Er, it has a serial number in the periodic table 68, density 9.06 g/cm^3, the atomic weight 167.26 and its electronic configuration is $4f^{12}6s^2$ (fig. 8).

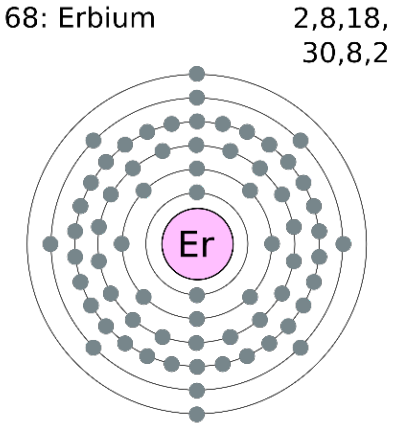

Figure 8. Electronic configuration of the erbium [Wi, 05].

The transition probability between 4f states is very sensitive to the ions which are around the RE chemical element [Mi, 91].

Erbium oxide is pink powder. Erbium lasers manufactured using erbium oxide are widely used in the medicine (in particular, in surgical interventions, because erbium has the ability to transmit energy without heating the tissues), dentistry and dermatology. Erbium monocrystals are widely used as high-performance laser materials.

Er^{3+} and Yb^{3+} codoped glasses have also attracted attention; Yb^{3+} ions play the role of the sensitizers that could absorb IR radiation and make a non-radiative transfer of extra energy

to Er^{3+} ions, that act as activators producing visible or UV upconversion luminescence. Absorption of a photon by Yb^{3+} ions leads to the transition from the ground state $^2F_{7/2}$ to the exited state $^2F_{5/2}$ (fig. 9), and then Yb^{3+} ions transfer energy to Er^{3+} ions exciting them to the level $^4I_{11/2}$. Thereafter the Er^{3+} ions have a non-radiative transfer resulting to an inverse distribution, which is formed between $^4I_{13/2}$ and $^4I_{15/2}$ states, and thus leading to the emission in IR range [Ba, 06]. Yb^{3+} and Er^{3+} energy diagram are shown in fig. 9.

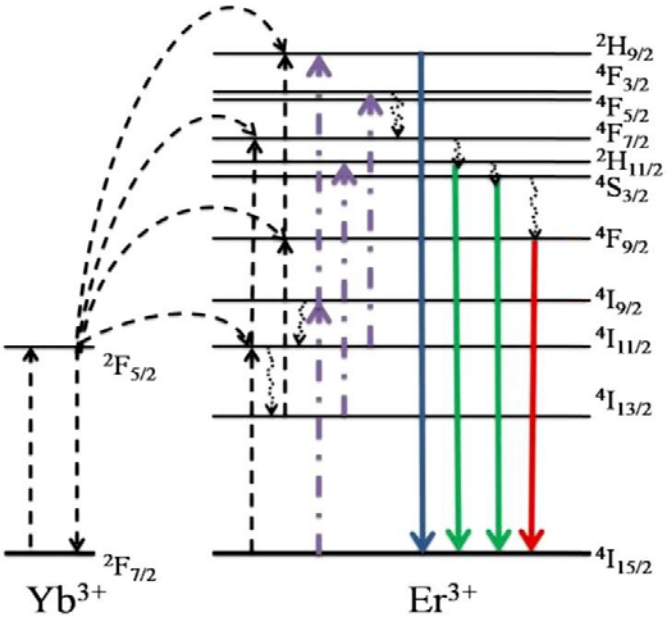

Figure 9. Energy diagram of Yb^{3+} and Er^{3+} ions: dashed lines from the Yb^{3+} show the energy transferring to the Er^{3+} [Ti, 14].

The main aim of developing fiber systems operating over an ultra-wide band (going from 1300 to 2000 nm) would demand the use of the different RE elements and glass matrices [Ba, 06].

Upconversion (UC) emission is a nonlinear effect where few IR photons are absorbed and converted into one, having higher energy ranging from UV to NIR. Three types of processes causing UC are presented on the fig. 10.

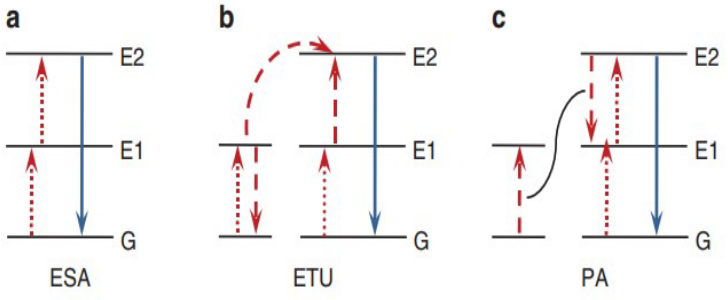

Figure 10. Scheme of the three types of processes causing UC in RE doped materials: a) excited state absorption (ESA); b) energy transfer upconversion (ETU); c) photon avalanche (PA) [Ac, 12].

ESA process can occur when two photons are absorbed by a single ion (fig. 10a). First photon causes excitation to metastable state (E_1), while ion is on the ground state (G). After that, second photon is absorbed and this process leads to transferring the ion from E_1 state to E_2 with higher energy. Finally, emission from the E_2 to G occurs.

ETU process (fig. 10b) shows two adjacent ions, which are excited by absorption of the photon (from G to E_1). The excited state energy from first ion is transferred to second ion also in state E_1. Donor ion goes to its G level while second ion promoted to level E_2. At final step, emission from E_2 to G occurs.

PA process occurs when it has certain pump intensity (fig. 10c). At first, the ion is excited to E_1 through weak non-resonant absorption of photon. It happened when adjacent ion undergoes ESA and excited to E_2. Next, cross-relaxation energy transfer to the adjacent ion in its ground state results in both ions occupying E_1. After that, resonant ESA and cross-relaxation energy transfers exponentially increase the population on the state E_2 and UC emission intensity [Ac, 12].

2.2 Optical fibers

2.2.1 Definition of the optical fibers

Optical fiber is composed of a glass core surrounded by a glass used as the cladding with lower value of refractive index (fig. 11).

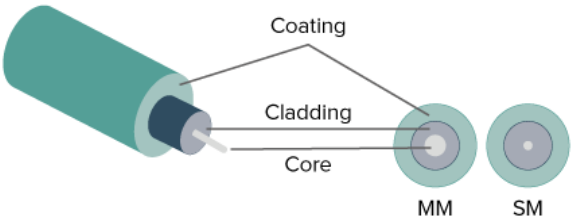

Figure 11. Schematic view and cross section of a fiber; MM – multimode, SM – single-mode [Os].

The polymer coating protects fiber from the physical and environmental damage [Th, 07]. The presence of the cladding increases the total internal reflection (TIR) of the core. TIR effect occurs when ray strikes the core-clad interface at an angle of incidence greater than the critical angle (θ_c in fig. 12) which is the angle of incidence for which a ray of light, while moving from a denser to a rarer medium, gazes over the surface of separation of two media [Pe, 16].

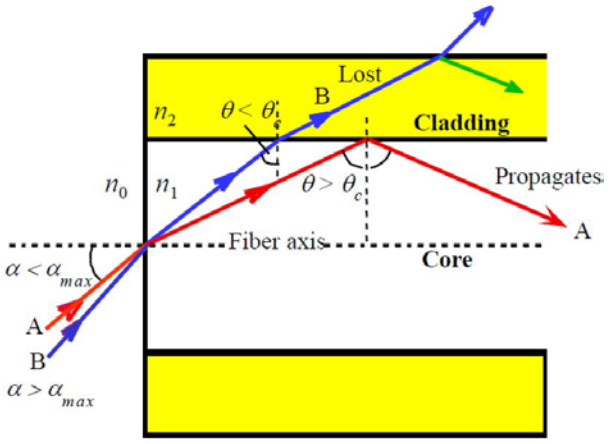

Figure 12. Snell's law: reflection and refraction on the example of fibers [Ka, 99].

Due to TIR, light travels inside the core and reflects from the walls. Walls absorb only small amount of the light from the core allowing the light beam to travel large distances. Some signal degradation occurs because of imperfections in the glass structure such as inhomogeneous structure (due to heat and composition), crystals, not melted particles from raw material, bubbles, cracks (due to thermoshock), stress (due to: heat, too fast cooling rate, mechanical process) [Du, 03] [Pe, 17a].

The best optical fibers show very little light losses, less than 10% per kilometer at 1550 nm. Cladding helps to keep the value of the critical angle constant through all length of the fiber and acts like a mirror that continually reflects the light ray along its path in the core

even across twists and turns. Maximum light losses occur at the points with maximum curvature (fig. 13).

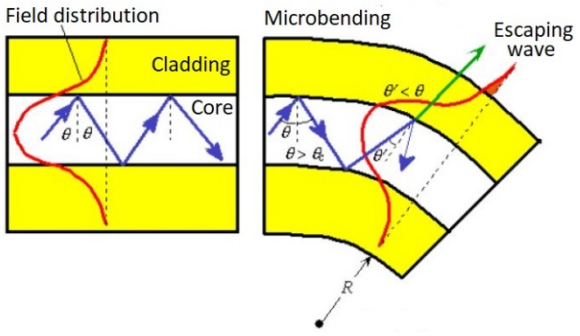

Figure 13. Losses on fiber bends [Ka, 99].

Sharp bends change the local waveguide geometry and waves are escaping from the fiber. Zig-zag beam with angle θ' gives rise to the transmitted wave, the field reaches the outside medium and some amount of the light is lost [Ka, 99].

Optical fibers could be single-mode, multimode or may not have a core (coreless fiber) and air will somehow act like a cladding with lower refractive index (as shown in fig. 14).

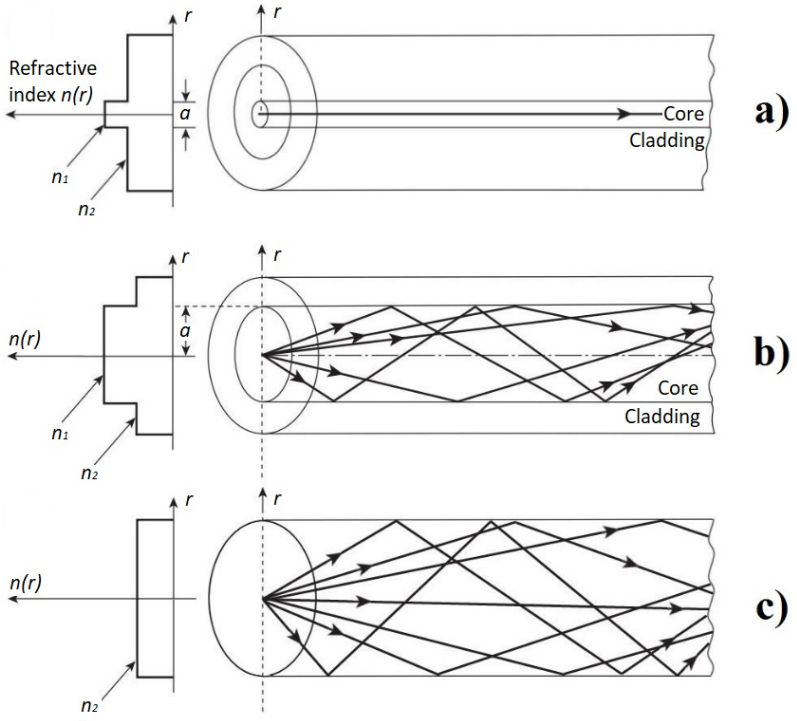

Figure 14. The refractive indexes of core and cladding and propagation of the ray in the: a) single-mode; b) multimode; c) coreless [Se, 09].

Single-mode fiber (SMF) is a fiber with small core diameter (usually up to 10 μm) which allows propagating only one transverse mode inside the core. Multimode fiber (MMF) has a TIR on the core-clad surface, so ray propagates like a zig-zag through the core. Usually, core diameter for MMF is 50 μm, so many modes could be inside the core [Se, 09].

2.2.2 Fabrication process and materials

Optical fibers are made from glasses with different refractive indexes. Fibers can be drawn from melt and/or from preform. The preform is melted and after annealing it is pulled to form of a long and thin optical fiber. Different methods can be used to prepare preforms:

Extrusion: this method is pretty simple; the core material is pressed through the sleeve with a cladding material on the bottom. Both materials are heated until they become soft enough to be pressed by a hydraulic plunger with needed pressure for that process (fig. 15). On the exit of the sleeve, an extruded cane, which could be used as a preform, is obtained.

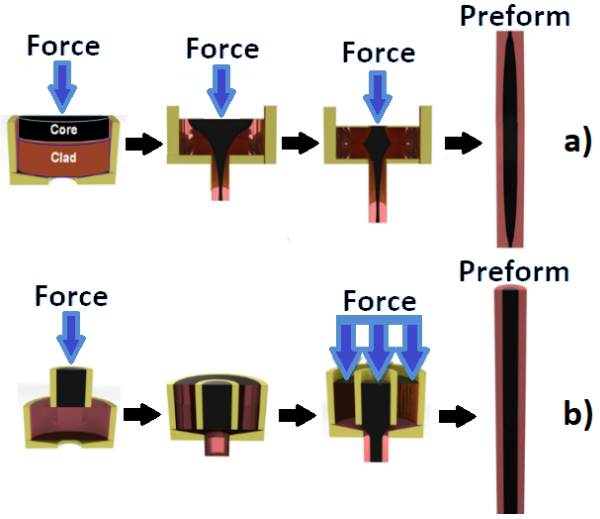

Figure 15. Extrusion of the preform through the sleeve: a) typical process when the fiber core distribution in the cladding is not uniform; b) new method, where barrier helps to keep ratio of materials constant [Ji, 16].

Chemical vapor deposition: this is a process where a solid material is deposited from a vapor by chemical reactions on the heated surface or near it. This method uses a mixture of gases which reacts with a flame to form hot glass soot by hydrolysis. This process is called soot process. Outside vapor deposition (OVD) and modified chemical vapor deposition

(MCVD) are different fabrication processes based on chemical vapor deposition systems. They are illustrated in Figure 16 a and b respectively.

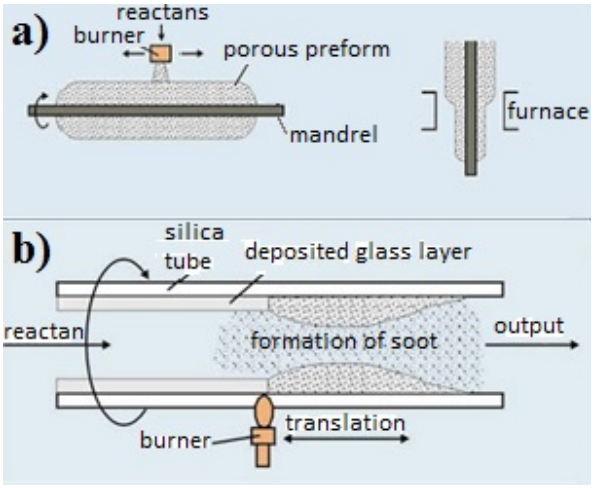

Figure 16. Schematic representation of the: a) OVD and b) MCVD processes [Dy].

In OVD, the mandrel is rotated usually at a speed of the 60 rotations in minute during the deposition. In MCVD, few layers of SiO_2 particles are deposited on the inside surface of the tube. Then mixture of the gases ($SiCl_4$, $GeCl_4$, O_2) is applied in the rod and when this mixture is placed in contact with the hot surface (flame is controlled by burner), particles start to fuse and glass layer is deposited.

Crucible method: this method is also called as direct melt method. The powder of the core material is placed in a vial, which is sealed at the bottom (fig. 17). Then the sealed vial with the powder is heated in the furnace to obtain a core preform. After that step, it could be pulled into the fiber. Nowadays double crucible method is widely used for fiber fabrication.

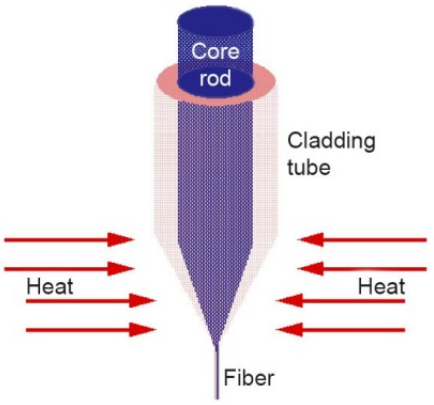

Figure 17. Schematic presentation of the crucible method [In, 19].

Rotational casting: this method (fig. 18) consists in the separate preparation of the core and cladding melts. The clad melt is quenched in a cylindrical mold which is spun at high speed (about 3000 rotations per minute) to obtain the tubular form. Then the molten core is quenched into the cladding.

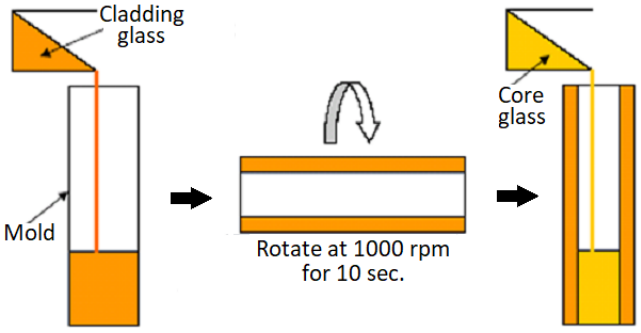

Figure 18. Schematic presentation of the rotational casting with vacuum pumping [Ma, 09].

The last step is fiber drawing. The preform is installed in a drawing tower (fig. 19).

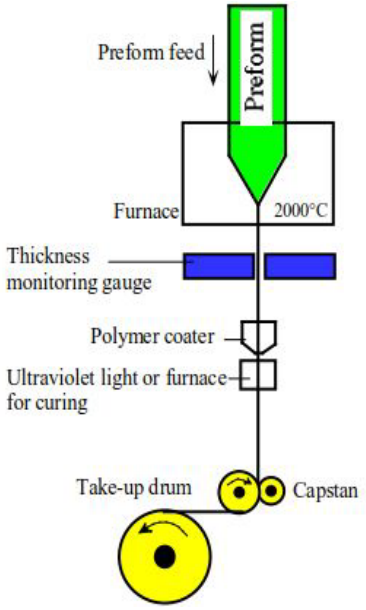

Figure 19. Scheme of the fiber drawing process [Ka, 99].

The drawing process goes in few steps: furnace, diameter regulation (thickness monitoring), coating and curing, winding fibers on the drum. The end part of the preform is heated and a drop of glass is formed. The fiber goes to the regulator, which allows the measurement of the fiber diameter during the drawing allowing one to maintain the diameter to the target value. If there is a laser regulator of the diameter, it is working in tandem with a tension detector: when the fiber diameter increases, the laser detector sends

a signal to the tension detector. Tension detector increases then the tension force, which leads to a decrease in the fiber diameter. To protect the optical fiber from the mechanical damage, a primary buffer coating is applied to the fiber surface, which is cured using UV lamp and/or heat.

2.2.3 Applications of the optical fibers

There are three major applications for the optical amplifiers in the modern optical networks, which use optical fiber as a medium: power amplifiers (which are placed directly after the laser diode transmitter), in-line amplifiers (also known as repeaters) or preamplifiers (which are placed before detector; the main goal of the preamplifier being to enhance the sensitivity of the detector).

In fig. 20 is schematic representation of the erbium doped fiber amplifier (EDFA) which has wide application in the field of telecommunications.

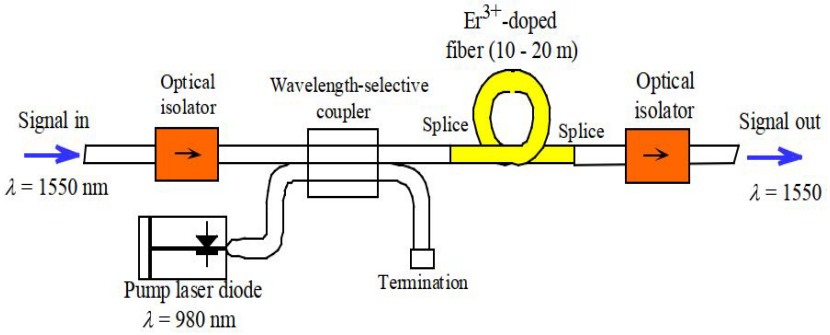

Figure 20. Erbium-ion doped fiber amplifier [Ka, 99].

With the discovery of lasers and their coupling with optical fibers, many fields started to use fibers in their procedures such as surgery, diagnostics, therapy and sensing. Lasers with Er^{3+}-doped fiber work at eye-safe wavelengths above 1.4 μm, thus light cannot damage human eyes.

Fibers are also extensively studied as sensors to detect molecules using evanescent principles. Nowadays, fiber evanescent wave spectroscopy (FEWS) is widely studied. FEWS provided promising results for the medical diagnostics. Evanescent waves from fibers are formed when sinusoidal waves are reflected in the TIR process (fig. 21).

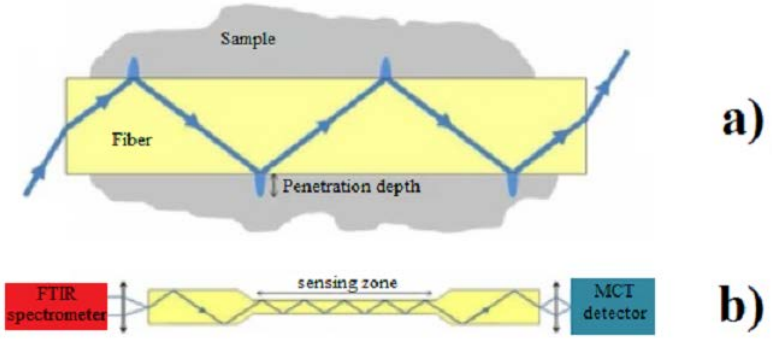

Figure 21. Fiber evanescent wave spectroscopy: a) mechanism of the process; b) setup and scheme of the tapered fiber [Bu, 14].

FEWS technique is quite simple and requires standard FTIR spectrometer, mercury cadmium tellurite (MCT) detector and fiber for the setup. To improve the sensing properties of the sensor, fiber diameter could be reduced locally – to create a tapered sensing zone (fig. 21b), which will be in contact (fig. 21a) with the sample to detect. Evanescent wave intensity decreases exponentially with distance from the fiber surface. Because of that fact, sensitive zone in FEWS is located within 1 μm from the surface of the fiber. Main application is in medical diagnosis; FEWS can detect and characterize presence of proteins, nucleic acids and lipids [Bu, 14] [Cu, 13].

3. EXPERIMENTAL PART

In the experimental part, the fabrication of the fibers investigated in this study is explained as well as the different techniques used to characterize the fibers and to test their sensing properties.

3.1 Fiber fabrication

In this work, 4 different fibers with a diameter of 125 μm were investigated. Their composition along with the label used in this study are listed in the table 1.

Table 1. Codes and compositions of investigated fibers.

Code	Composition (in mol%)
Er REF	$82.8NaPO_3$-9.2NaF-5ZnO-$2.5Ag_2O$-$0.5Er_2O_3$
Er HT	$82.8NaPO_3$-9.2NaF-5ZnO-$2.5Ag_2O$-$0.5Er_2O_3$
Er, Yb REF	$49P_2O_5$-39.2SrO-$9.8Na_2O$-$0.5Er_2O_3$-$1.5Yb_2O_3$
Er, Yb NPs	$2.5NaYF_4$ ($83.25NaPO_3$-9.25NaF-5ZnO-$2.5Ag_2O$)

The Er REF fiber was drawn from a preform. The raw materials used to prepare the preform were $(NaPO_3)_6$ (Alfa Aesar, 99.99%), NaF (Sigma-Aldrich, ≥ 99.0%), ZnO (Sigma-Aldrich, ≥ 99.5%), Ag_2SO_4 (Sigma-Aldrich, 99.999%) and Er_2O_3 (MV Laboratories Inc., 99.5%). Two preforms were prepared. The 35 g batches were melted in a quartz crucible for 5 minutes at 875 °C. After quenching, the preforms were annealed at 200 °C for 6 hours to release the stress from the quench. One of the preforms was heat treated at 10 °C above its glass transition temperature for 17 hours to precipitate Ag nanoparticles (Er HT fiber). Prior to drawing, the surface of the preform was polished. The fibers were drawn using a drawing temperature of 410 °C. The feed rate was 1.5 mm/min and the drum speed was 6.22 m/min.

The Er, Yb REF fiber was also drawn from a preform. The raw materials used to prepare the preform were $NaPO_3$ (Alfa Aesar, 99.99%), Er_2O_3 (MV Laboratories Inc., 99.9%) and Yb_2O_3 (Sigma-Aldrich, 99.9%). The $Sr(PO_3)_2$ precursor was independently prepared using

$SrCO_3$ and $(NH_4)_2HPO_4$ as raw materials and with heating up to 850 °C. The 25 g batch was melted for 45 minutes at 1150 °C and then casted in a 11 cm long graphite mold with a diameter of 1 cm, preheated at 300 °C. After quenching, the preform was annealed at 400 °C for 10 hours to decrease the residual stress. The fiber was drawn using a drawing temperature of 550 °C in He inert atmosphere. The feed rate was 2 mm/min and the drum speed was 10 m/min [Gu, 17].

The Er, Yb NPs fiber was drawn from a preform. The raw materials used to prepare the preform were $(NaPO_3)_6$ (Alfa Aesar, 99.99%), NaF (Sigma-Aldrich, ≥ 99.0%), ZnO (Sigma-Aldrich, ≥ 99.5%), Ag_2SO_4 (Sigma-Aldrich, 99.999%). Preform of 20 g batch were melted at 750 °C for 5 minutes and then placed at doping temperature of 550 °C for 20 minutes, after that $NaYF_4$: Er^{3+}, Yb^{3+} nanoparticles were added and 3 minutes later the glass was casted inside the mold [Oj, 18]. The synthesis of $NaYF_4$: Er^{3+}, Yb^{3+} can be found in [La, 15]. Prior to drawing, the surface of the preform was polished. The fiber was drawn using a drawing temperature of 405 °C. The feed rate was 1 mm/min and the drum speed was 6.18 m/min.

3.2 Thermal properties of fibers

The thermal properties of the glasses were measured using NETZSCH STA 449 F1 Differential Scanning Calorimetry (DSC) (fig. 22).

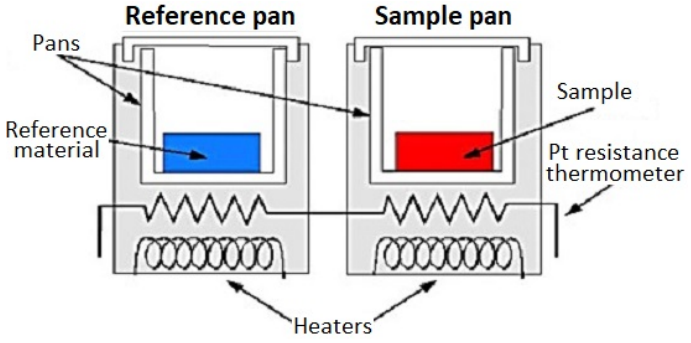

Figure 22. Scheme of the DSC installation [Le, 13].

The measurement was performed by heating ~30 mg of the glass crushed into powder in Pt-Rh crucible up to 700°C with heating rate 10°C/min. Reference crucible (blue in fig. 22) needed to be empty.

The measurement consists of measuring the difference in the absorbed heat energy between the sample and the reference, the heat flow that corresponds to the amount of power input in Watts needed to increase the temperature of 1 mg of sample by 1°C. All measurements were done in a N_2 flux (20 ml/min).

An example of a thermogram is presented in fig. 23.

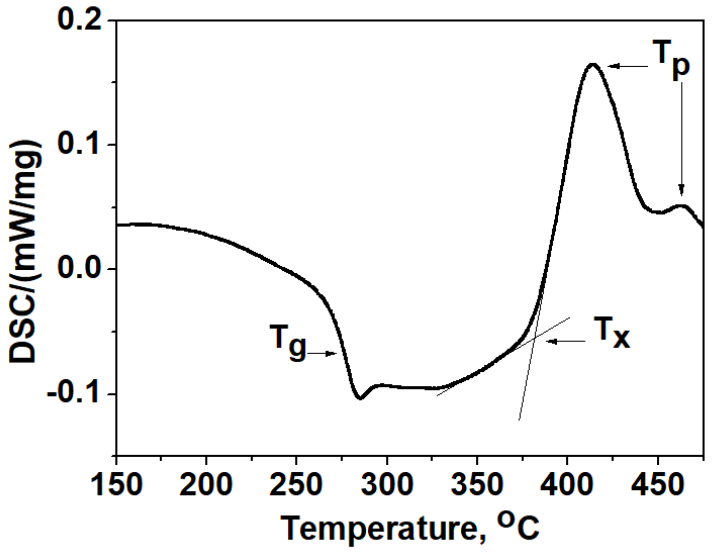

Figure 23. Thermogram of Er HT preform taken as an example.

T_g is a glass transition temperature and it is determined as the inflection point of the endotherm obtained by taking the first derivative of the DTA curve, while T_x and T_p (crystallization temperature) were taken at the onset and at the maximum of the exothermic peak, respectively. The accuracy of the measurement is ±3°C.

Value of $\Delta T = (T_x - T_g)$ can be then calculated. It is a useful criterion for evaluating the thermal stability of glass. A ΔT larger than 100°C is a clear indication that the glasses are stable against crystallization and therefore good glass candidate for fiber drawing.

3.3 Scanning electron microscope

The geometry of the fiber was checked using a scanning electron microscope (SEM) – Carl Zeiss Crossbeam 540 depicted in fig. 24.

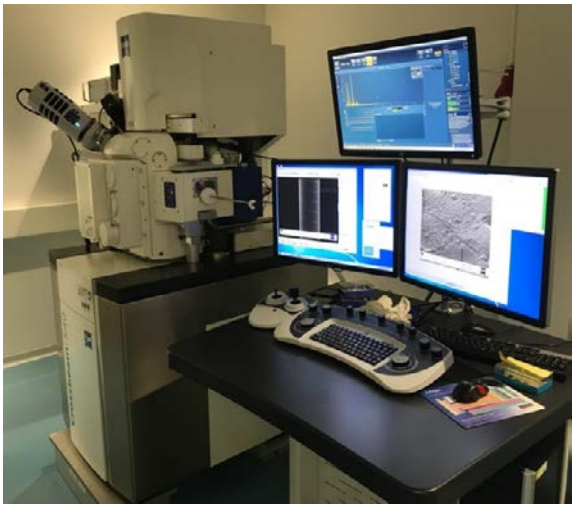

Figure 24. SEM/EDS installation in Tampere University.

The schematic of the SEM is shown below.

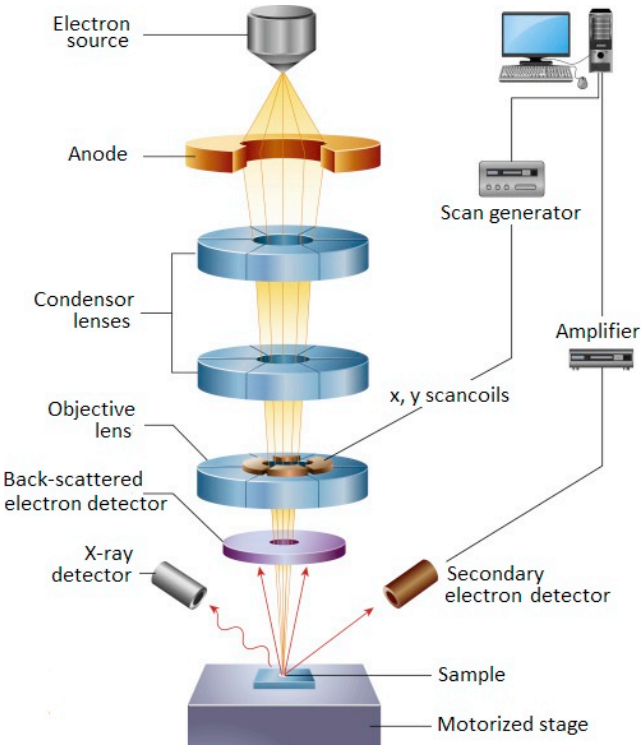

Figure 25. Scheme of the SEM installation [In, 16].

Electron source (also known as an electron gun) produces electron beam and this beam travels down through the column with different equipment. Condenser lenses focus the electron beam while it moves down; objective lens has scanning coils on it. Scanning coils are used to deflect the electron beam in x and y axes. After these lenses and coils, there are backscattered electron detector and secondary electron detector.

- Backscattered electron (BSE) detector detects elastically scattered electrons (backscattered electrons), which carry the information about composition of the sample. Carrying data about sample composition becomes possible because of the interactions between the elements from the sample and the electron.
- Secondary electron (SE) detector detects inelastic interactions of electrons (secondary electrons) and leads to topography images with resolution independent of material. Scattering of SE is inelastic because primary electrons from beam are losing energy while they eject electron from the sample and this energy is transferred to the electrons from the sample surface.

When the electron beam displaces the electron of the inner shell (which is replaced by the electron of the outer shell), an x-ray is emitted. Since each element from the periodic table has a unique energy difference between the outer and inner shells of the electrons, the detected x-rays provide elemental identification. This elemental dispersive spectroscopy data can be obtained at a point or mapped over some area. In fig. 26 scheme of the electron beam interactions is presented.

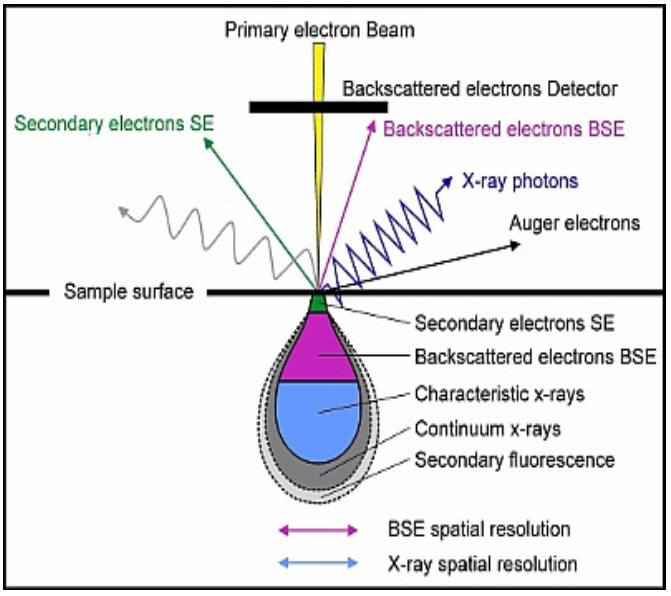

Figure 26. Scheme of the electron beam interactions [Gl].

In this study, the fibers were coated with conductive material in Jeol JEC-530 auto carbon coater to be able to obtain image of the fibers. The coating also improves the image contrast. Accuracy of the measurement is 1 μm.

The semi-quantitative elemental analysis of the composition of the fiber samples was done by using the Oxford Instruments X-Max^N 80 Elemental dispersive X-ray spectroscopy (EDS) detector. Accuracy of the measurement is ±1.5 mol%.

3.4 FTIR spectroscopy

The structural analysis of the samples was done using infrared (IR) spectroscopy. The samples were crushed into powder for the measurement. The IR spectra of the powder from fibers were measured using a Perkin Elmer Spectrum FTIR2000 spectrometer with Attenuated Total Reflectance (ATR) mode in mid IR region between 600 and 1400 cm^{-1}. The resolution of measurements was 2 cm^{-1}, spectra were obtained from accumulation of eight scans.

The principle of IR spectroscopy lies in the study of the interaction of IR radiation (range is shown on the fig. 27) with the sample.

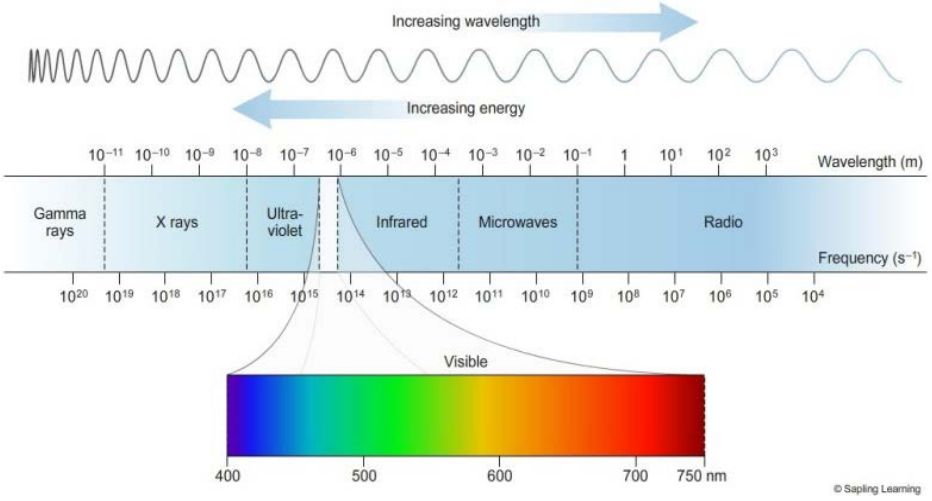

Figure 27. Electromagnetic spectrum and visible light [Al].

When IR radiation passes through the sample, atoms are excited and begin to oscillate. While atoms are oscillating, a decrease in the intensity of the light passing through the sample is observed. This absorption occurs at those wavelengths, the energy of which corresponds to the excitation energies of oscillations in the atoms. Thus, the wavelength with the maximum absorption of IR radiation can show the presence of certain fragments in the sample. This is widely used to establish the structure of the glass.

FTIR spectrometer is made of a coherence light source (IR), a beam splitter (half-silvered mirror), one stationery and one moving mirror, a sample chamber and a photoelectric detector or camera. The schematic representation of the FTIR installation is presented in fig. 28.

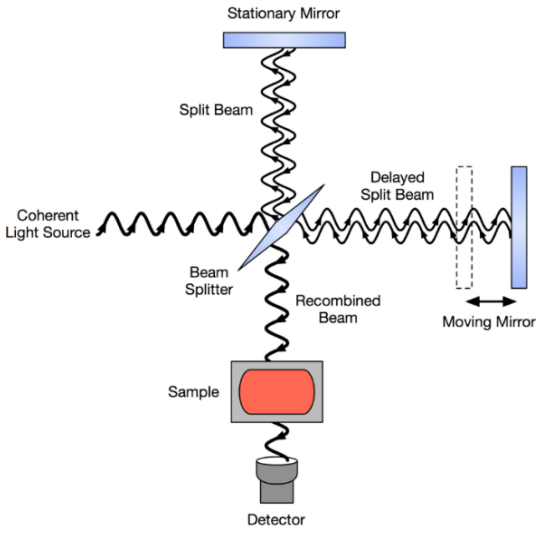

Figure 28. Scheme of the FTIR spectroscopy setup [Wi, 11].

Using a beam splitter, a light beam splits into two rays – one part transfers to the stationary mirror and second goes to the moving mirror. Each of those light beams is reflected back toward the beam splitter, which then combines their amplitudes using the superposition principle. Distance between beam splitter and moving mirror can be changed and this change will affect interference of beams. The resulting interference pattern is typically directed to photoelectric detector or camera (not directed back toward the source). Finally, the sample is placed between beam splitter and detector. The sample absorbs different wavelengths and detector collects that information in the form of interferogram, energy versus time signal. Fourier-transform function is used to convert this resulting interferogram into intensity as a function of wavelength.

3.5 Optical properties

Fig. 29a shows physical process of the emission spectroscopy and fig. 29b shows up- and downconversion mechanisms.

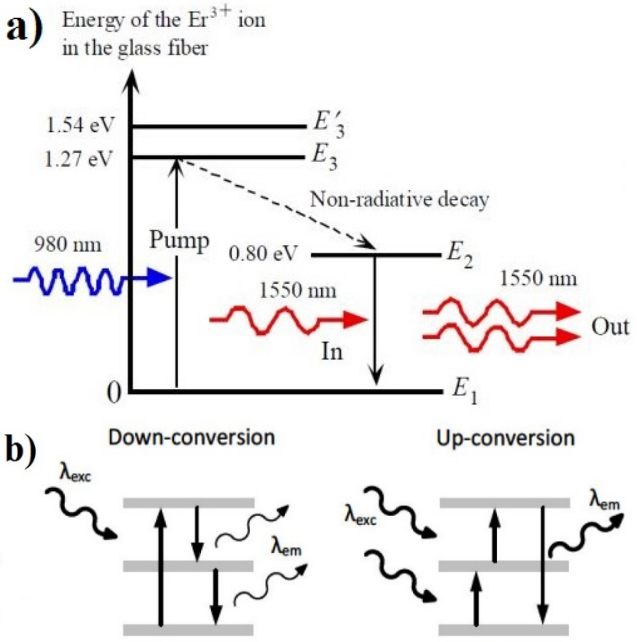

Figure 29. a) Energy diagram for the Er^{3+} ion in the glass fiber medium and light amplification by stimulated emission from E_2 to E_1 [Ka, 09]; b) downconversion and upconversion mechanisms [St, 07] [St, 16].

When atom is excited it transfers from ground state to a higher energy level. Excitation could be caused by collision with electron or photon, which gives its energy to an atom's electron. After being excited, electron will come back to the ground state and during this transition, energy difference between two states will be emitted in the form of photon (equation 1). Emission spectroscopy is a method, which examines wavelengths of photons emitted during transferring from excited state to state with lower energy. Fig. 29a shows, that using excitation of 980 nm it is possible to obtain 1.55 μm emission spectrum for Er^{3+}. Fig. 29b shows scheme of upconversion (UC) and downconversion (DC) processes of the Er^{3+}. DC process is a process where emitted photon has lower energy than absorbed photon; most emission processes in nature are DC and this effect appears because of the losses due to vibrational relaxation (Stokes shift). Opposite to this effect is UC. Mechanisms to achieve UC luminescence include absorption within a single-doper ion and different energy transfers from excited states (see fig. 10).

The measurement of the optical properties consists of measuring the absorption and emission spectra (visible and NIR). Schemes of homemade set up presented in fig. 30.

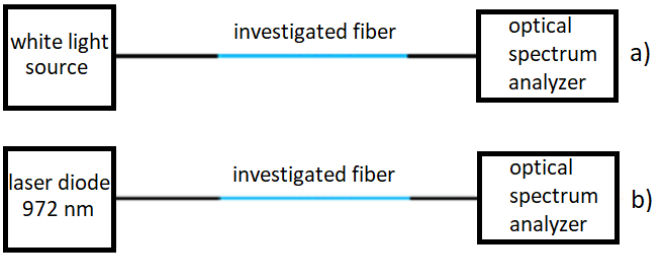

Figure 30. Scheme of the setup used for the absorption (a) and emission (b) measurements.

The investigated fibers were set on the fiber holder and fixed with an adhesive tape. Conventional magnetic clamps, which are usually used for fixation, could not be used here because of the fragility of the investigated fibers. It should be reminded that the fibers were not coated with a polymer buffer.

The investigated fibers with different lengths (ranging from 1.2 to 5 cm) were coupled to the light source and the optical spectrum analyzer (OSA) using two multimode silicate fibers (fig. 31). Excitation beam goes from left to right.

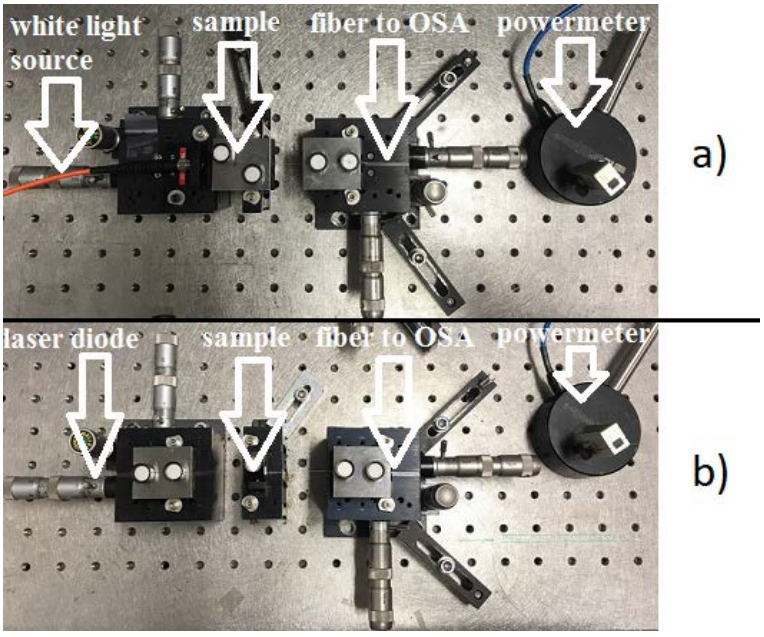

Figure 31. Picture of the setup used for the absorption (a) and emission (b) measurements in Tampere University.

For the absorption spectra measurements, the light transmitted through the investigated fiber was measured in continuous mode using a Thorlabs SLS201/M white light source. Maximum output was measured by ILX Lightwave 0MM-6810B optical multimeter with

ILX Lightwave 0MH-6703B power head (wavelength range from 400 to 1100 nm). Spectra were obtained using an optical spectrum analyzer (ANDO AQ-6315A) with a wavelength range from 350 to 1750 nm.

The emission spectra were obtained by exciting the optical fiber with a laser diode operating at 972 nm excitation. Maximum output from the investigated fiber was also measured by ILX Lightwave 0MM-6810B optical multimeter and spectra were obtained by an OSA ANDO AQ-6315A. To detect upconversion in visible range Avantes AVASPEC OSA was used.

3.6 Testing sensing properties

The main aim of this study was to test the sensing properties of the investigated optical fibers when in contact with N-Methylaniline (NMA). NMA is a toxic chemical for synthesis, which is produced by Merck KGaA, Darmstadt, Germany. Chemical formula of the NMA is $C_6H_5NHCH_3$, molar mass is 107.16 g/mol and pH is 7.6. The NMA is in liquid state at room temperature with a yellow color, its odor is sweet; it is possible to make solutions of the NMA with pure ethanol, but not with water because of the oily condition of the NMA.

The emission spectra of the fibers in contact with NMA were obtained by exciting the investigated fiber with a laser diode operating at 972 nm excitation. Maximum output from the fiber was measured using ILX Lightwave 0MM-6810B optical multimeter and the emission spectra were recorded using an optical spectrum analyzer ANDO AQ-6315A.

5 cm long fibers were immersed in 2 ml of solutions containing a mixture of Ethanol/N-Methylaniline with different ratios. A schematic of the mold used for the immersion is shown below (fig. 32).

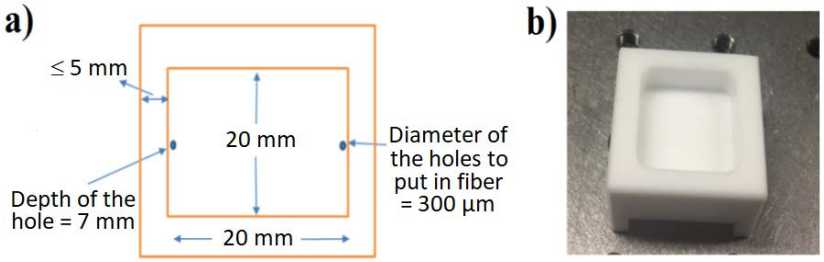

Figure 32. Mold used for the measurements: a) scheme of the mold with dimensions; b) image of the mold.

The emission spectra were recorded using the set up shown in the fig. 33.

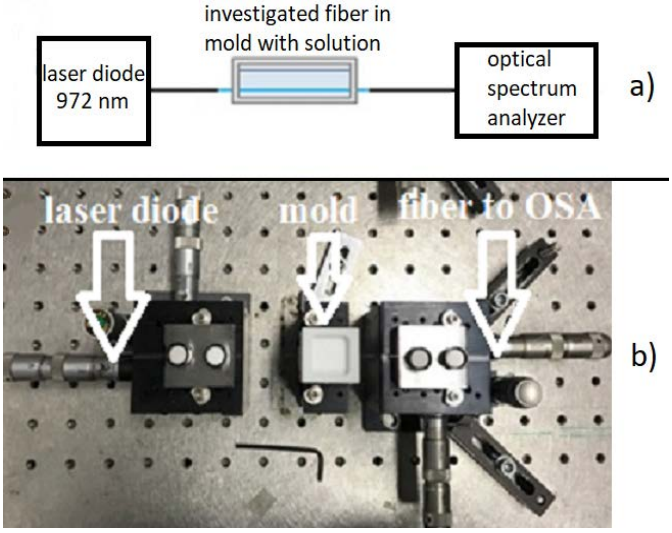

Figure 33. Setup used for the emission measurements with NMA solutions: a) scheme; b) real installation in Tampere University.

Drops of the mixture of Ethanol/NMA with different ratios were also deposited at the surface of 1.5 cm long fibers as shown in fig. 34.

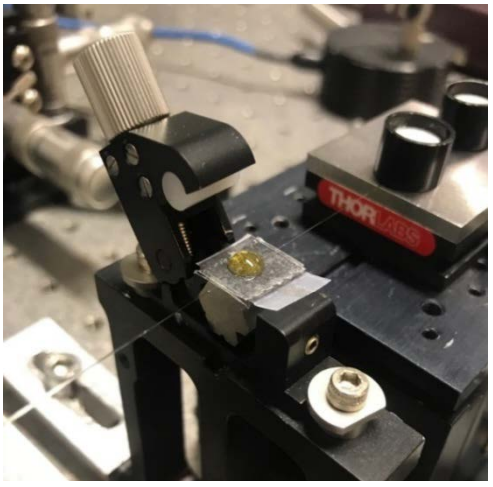

Figure 34. Picture of the setup used to measure emission spectra of 1.5 cm long fiber in contact with 2 drops of mixture of Ethanol/NMA in Tampere University.

4. RESULTS AND DISCUSSION

Four fibers listed in Table 1 were investigated in this study.

Fiber was successfully drawn from the glass preform with the composition $82.8NaPO_3$-$9.2NaF$-$5ZnO$-$2.5Ag_2O$-$0.5Er_2O_3$ (in mol%). This fiber is labeled here as **Er REF fiber**.

In order to create Ag nanoparticles in the Er REF fiber, a preform with the same composition was prepared and heat treated at 10 °C above its glass transition temperature for 17 hours prior to drawing. This fiber is labeled **Er HT**.

Fiber was also drawn from a glass with the composition $83.25NaPO_3$-$9.25NaF$-$5ZnO$-$2.5Ag_2O$ (in mol%) which contains also 5 wgt% of $NaYF_4$: Er^{3+}, Yb^{3+} nanoparticles. This fiber is labeled as **Er, Yb NPs**. As explained in [Oj, 18], this glass exhibits strong upconversion under 980 nm pumping from laser source due to the presence of the nanocrystals. However, the preparation of such fiber is challenging, as it is well known that not all the nanocrystals can survive in the glass melt as they decompose already at 750 °C during the preparation of the glass melting [Oj, 18]. However, it is not known if the fiber drawing process has an impact on the survival of the nanocrystals.

As the three fibers were drawn from glasses which are known to be hygroscopic due to their composition, because of the low amount of P_2O_5, fiber with the composition $49P_2O_5$-$39.2SrO$-$9.8Na_2O$-$0.5Er_2O_3$-$1.5Yb_2O_3$ (in mol%) was also investigated in this study and labeled here as **Er, Yb REF**. More detailed information about this fiber can be found in [Gu, 17].

As these fibers were drawn from new glass compositions, the fibers were drawn into 125 μm single core fibers without buffer coating. Therefore, the fibers are very fragile and hygroscopic. As the drawing process is known to lead to changes in the glass properties due to the severe quenching under the imposed drawing stress [Lu, 99], the thermal, optical and structural properties of the fibers are first presented before presenting the results of testing the sensing properties of the fibers.

4.1 Characterization of the fibers

Before testing the fibers, it is important to understand the impact of the fiber drawing on the thermal and structural properties of the glasses. The thermal properties of the glasses prior to and after drawing are presented in Table 2.

Table 2. Results for the DTA for fibers and their preforms

	T_g (± 3°C)	T_x (± 3°C)	T_p (± 3°C)	$\Delta T = T_x - T_g$ (± 6°C)
Er REF Preform	282	388	429, 475	106
Er REF Fiber	274	362	389, 434	88
Er HT Preform	278	380	414, 464	102
Er HT Fiber	270	343	384, 425	73
Er, Yb REF Preform*	462	580	593	118
Er, Yb REF Fiber*	456	578	594	122
Er, Yb NPs Preform	272	388	435, 476	116
Er, Yb NPs Fiber	275	340	391, 452	65

*Data from [Gu, 17]

Significant changes in the thermal properties of the glass after drawing can be observed for all investigated fibers; except for Er, Yb REF glass system. The T_g, T_x and T_p decrease after drawing as well as ΔT indicating that the glass becomes a poor glass former after drawing.

One can notice that the heat treatment of the Er doped glass does not lead to changes in the thermal properties of the preform and fiber. One should remind that the preform was heat treated at its (T_g + 10 °C) for 17 hours in order to grow Ag nanoparticles. After heat treatment, the color of the glasses changed from pink to yellow color, but the yellow color was only at the surface of the preform, indicating that the Ag nanoparticles are probably formed only on the surface of the glass. A study of the location of the Ag nanoparticles forming during heat treatment is ongoing. As all preforms were polished before drawing to

increase the surface quality of the fibers, the preform was pink as the Er doped preform used as a reference.

The IR spectra of the preforms and fibers are shown in fig. 35. They are normalized to the band with the highest intensity.

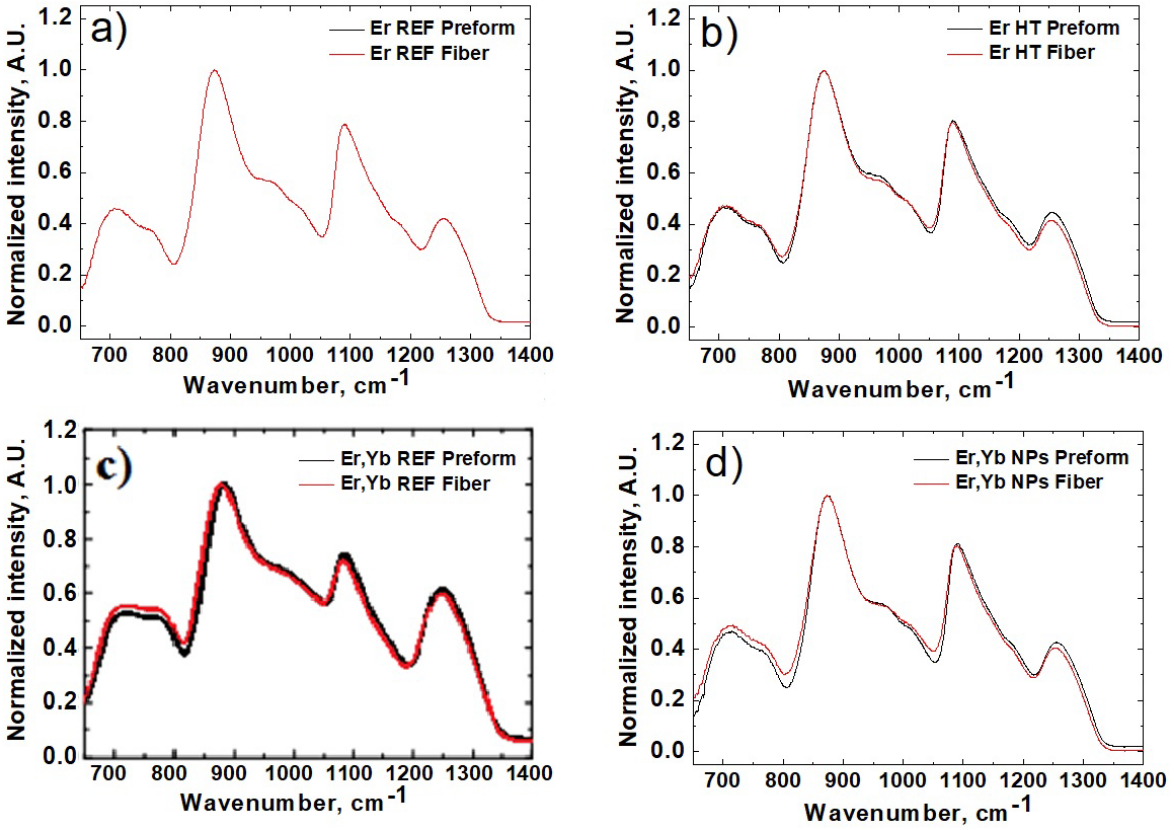

Figure 35. Normalized IR spectra of the preform and fiber of: a) Er REF; b) Er HT; c) Er, Yb REF [Gu, 17]; d) Er, Yb NPs.

The spectra in the fig. 35 exhibit bands at 650-800, 880, 1085 and 1250 cm^{-1}. The broad band from 650 to 800 cm^{-1} corresponds to symmetric vibrational modes of Q^2 phosphate (metaphosphate) units [Ko, 10] [Sh, 07b]. The main band at 880 cm^{-1} is related to the asymmetric vibrational mode in Q^2 units and the band at 1080 cm^{-1} to the asymmetric stretching vibrations of Q^2 and Q^1 units [Br, 94] [Ko, 10] [Sh, 07b]. The shoulders at ~950 and at ~1030 cm^{-1} are related to the asymmetric stretching vibrations of Q^2 units in small and large rings, respectively and the shoulder at 1154 cm^{-1} to symmetric vibration of PO_2 in Q^2 units, [Ab, 09] [Ga, 04a] [Wi, 84].

The shoulder at 980 cm^{-1} and the band at 1085 cm^{-1} can be associated with the symmetric and asymmetric stretching vibrations of the Q^1 phosphate unit, respectively [Ab, 09] [Ga, 04a] [Mo, 98] and the band at 1250 cm^{-1} with the asymmetric stretching mode of Q^2 phosphate units [Ga, 04a] [Ko, 10] [Me, 97] [Mo, 98]. The band at 1085 cm^{-1} can be also attributed to Q^2 groups in metaphosphate [Il, 01].

Independently of the glass composition, the drawing process leads to slight changes in the IR spectra indicating that minor change in the structure of the glass occurs during the fiber drawing. A slight decrease in intensity of the bands at 1085 and 1250 cm^{-1} occurs after drawing associated with a slight increase in intensity of the bands in the 650-800 cm^{-1} range. These changes tend to indicate that the fiber has weaker network connectivity with slightly less Q^2 units and probably reorientation of the P-O-P bonds compared to that of the bulk glass. Similar results were reported in [Gu, 17]. This change in the glass structure is in agreement with the decrease in the T_g after drawing and might be due to severe quenching under the imposed drawing stress [Lu, 99].

The IR spectra of the Er REF and Er HT preforms and fibers are shown in fig. 36a and b respectively. Spectra are normalized to the band with the highest intensity.

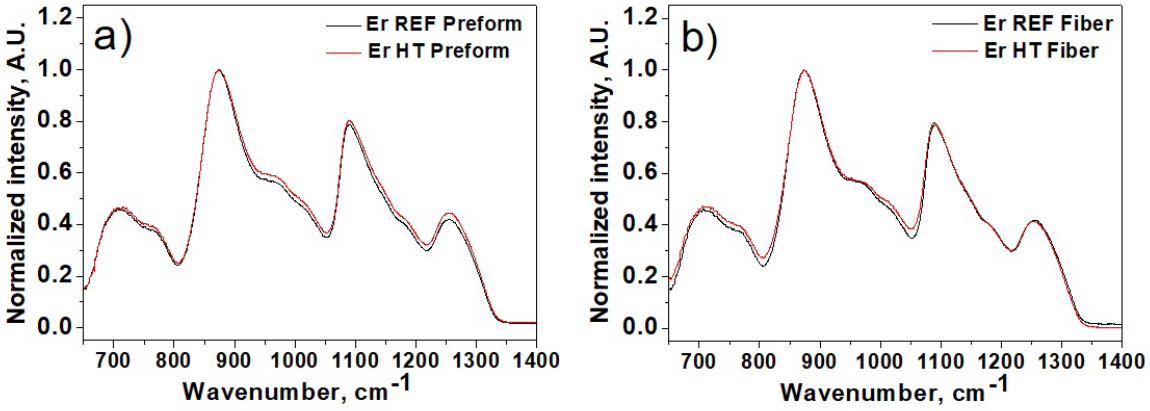

Figure 36. Normalized IR spectra of the Er REF and Er HT: a) preforms; b) fibers.

The IR spectra of the preform prior to and after heat treatment are similar: the heat treatment is thought to slightly increase the intensity of the band at 1250 cm^{-1} and of the shoulders at 950 and ~1150 cm^{-1}, indicating that the heat treatment increases the

connectivity of the glass network. However, after drawing, the fibers exhibit similar IR spectra. The thermal history of the preforms is erased by the drawing process.
The picture of the fibers taken with a SEM images can be found in fig. 37.

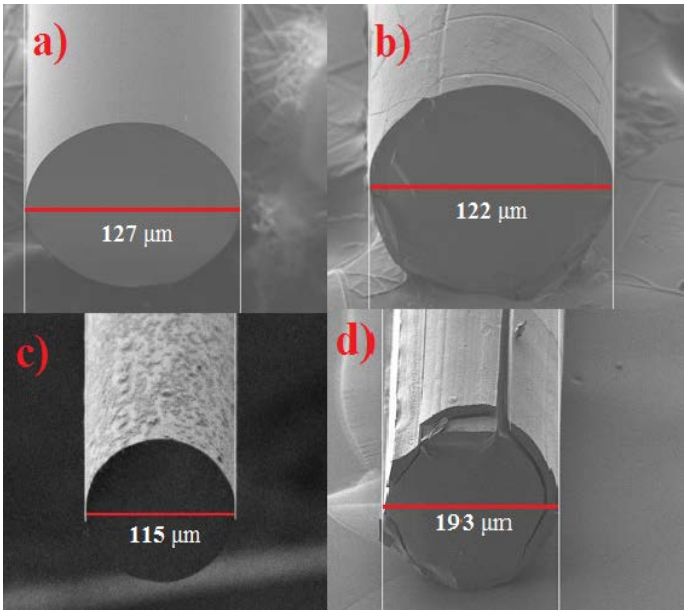

Figure 37. SEM image of the cross-section: a) Er REF fiber; b) Er HT fiber; c) Er, Yb REF fiber from [Gu, 17]; d) Er, Yb NPs fiber.

All fibers are circular and concentric. The Er REF fiber exhibits an almost ideal surface without significant scratches, whereas the surface of the Er HT fiber is not that smooth (as shown in fig. 37b). The scratches seen at the surface of the fibers are thought to come from the polishing. No Ag nanoparticles were found at the surface of the fibers. The diameter of the Er REF and Er HT fibers is (127±2) and (122±2) µm respectively, which is close to the expected 125 µm fiber diameter.

The diameter of the Er, Yb REF fiber is (115±2) µm, as reported in [Gu, 17]. The diameter of the Er, Yb NPs fiber is (193±2) µm, which is bigger that the targeted 125 µm fiber diameter. Additionally, one can notice that its surface is damaged: deep cracks were observed in all the pieces of the fibers (see fig. 38). We think that the bad quality of this fiber, compared to the other fibers, is due to its composition: indeed, its amount of P_2O_5 is the lowest and so this Er, Yb NPs glass is expected to be the most hygroscopic of the glasses of investigation and so the least stable glass after drawing.

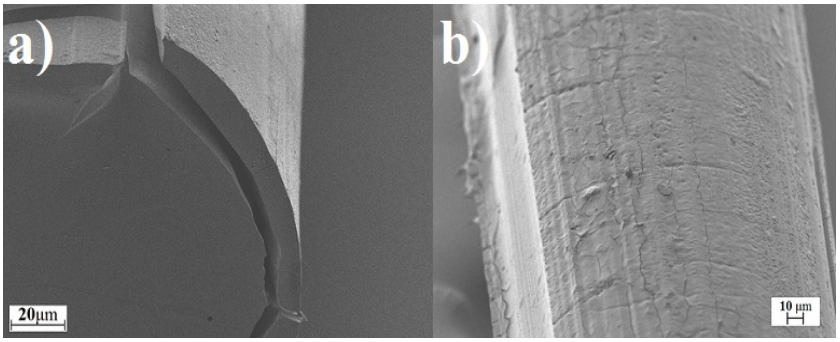

Figure 38. SEM image of the Er, Yb NPs fiber surface: a) separated layer and a hole; b) scratches.

The compositions of the investigated optical fibers were determined from the fiber surface by the SEM coupled with EDS are presented in table 3.

Table 3. EDS results for investigated fibers (±1.5 mol%).

	Na_2O	P_2O_5	NaF	ZnO	Ag_2O	Er_2O_3	Yb_2O_3	SrO
Theoretical composition Er REF fiber	41.4	41.4	9.2	5	2.5	0.5	-	-
Observed composition Er REF fiber	43.5	43.3	4.7	5.5	2.5	0.5	-	-
Theoretical composition Er HT fiber	41.4	41.4	9.2	5	2.5	0.5	-	-
Observed composition Er HT fiber	44.5	42.2	4.8	5.1	2.9	0.5	-	-
Theoretical composition Er, Yb REF fiber	9.8	49	-	-	-	0.5	1.5	39.2
Theoretical composition Er, Yb NPs fiber	41.6	41.6	9.3	5	2.5	-	-	-
Observed composition Er, Yb NPs fiber	47.4	39.4	5.1	5.2	2.9	-	-	-

As seen in Table 3, the fibers exhibit a lower NaF concentration than expected due to the low sensitivity of the SEM for fluorine while within the accuracy of the EDS measurement, composition of the Er, Yb REF fiber was found to be identical compared to the composition of the preform in [Gu, 17].

Nonetheless, according to the composition analysis, no dramatic changes in the composition of the glass is expected to occur during the fiber drawing in agreement with the changes in the thermal and structural properties already discussed. Finally, one can notice that the heat treatment of the preform does not lead to changes in the fiber composition, confirming that if Ag nanoparticles were formed during the heat treatment, they were probably removed during the polishing.

The absorption spectra of fibers are presented in fig. 39. Also smoothed spectra are shown. Smoothing was done by adjacent-averaging method. Firstly, smoothing was done only for Er, Yb NPs spectrum (fig. 39d), because it has noisy signal and it was hard to say anything about 400-600 nm region. After that, smoothing was also done for other absorption spectra.

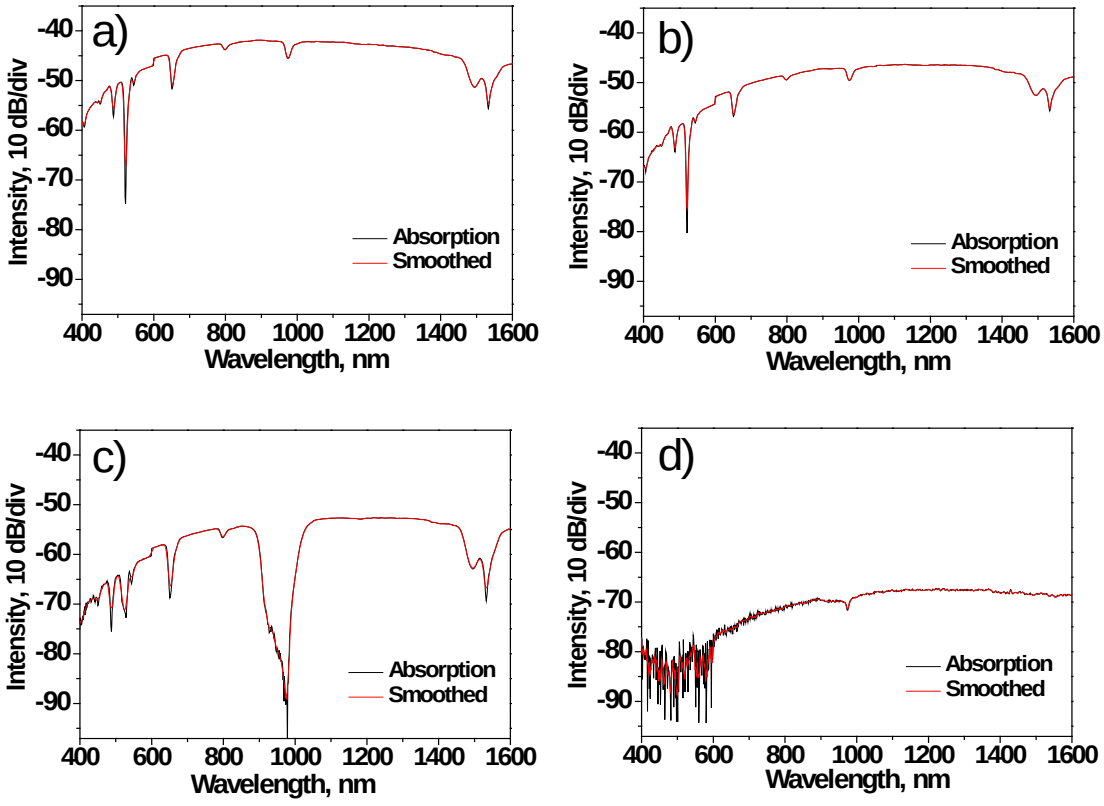

Figure 39. Absorption spectra of the: a) Er REF fiber; b) Er HT fiber; c) Er, Yb REF fiber; d) Er, Yb NPs fiber.

The absorption spectra exhibit several bands, which are characteristics of the Er^{3+} ion 4f-4f transitions from the ground state to various excited levels [Bu, 10]. Because it was not possible to cleave the fibers, it is not possible to compare the absorption (dB/div) of the

fibers. One can notice that the Er, Yb REF fiber exhibits an absorption band at 980 nm with the highest intensity (fig. 39c). This is due to the presence of Yb^{3+} ions, which exhibit a strong absorption band at 980 nm.

One should point out the absorption of the well-known absorption band at ~410 nm, which corresponds to the surface plasmon resonance absorption of Ag nanoparticles [Ga, 04b]. The shape of the absorption spectrum of the Er HT fiber confirms that the fiber is free of Ag nanoparticles.

As seen in fig. 39d, an absorption band at 980 nm with small intensity was detected confirming the presence of the Yb^{3+} in the glass. As seen in fig. 40, this absorption band is broad indicating that Yb^{3+} ions are most probably located in an amorphous site. As explained in [Oj, 18], some $NaYF_4$: Er^{3+}, Yb^{3+} crystals are thought to survive in the glass during the glass preparation. However, from the absorption spectra of the fibers, there is no evidence about the presence of the nanoparticles in the tested fibers.

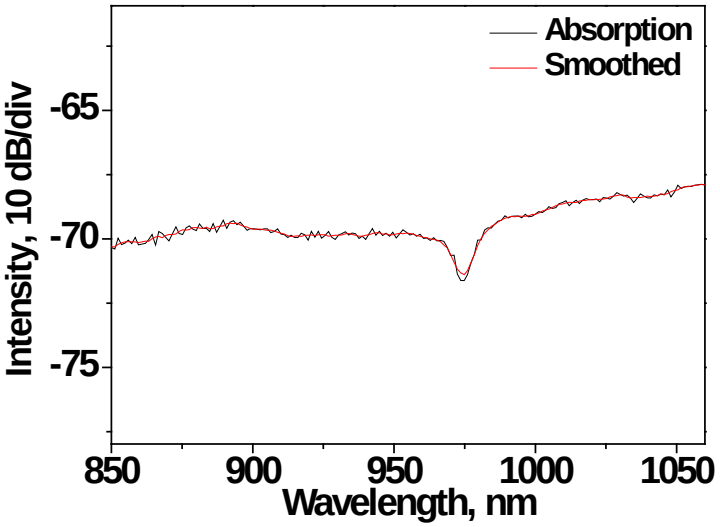

Figure 40. Absorption spectra of the Er, Yb NPs fiber at 980 nm, enlarged from fig. 39d.

The comparison of the absorption bands at 980 nm and 1.5 μm of the Er REF, Er HT and Er, Yb REF fibers are presented on the fig. 41a and b respectively.

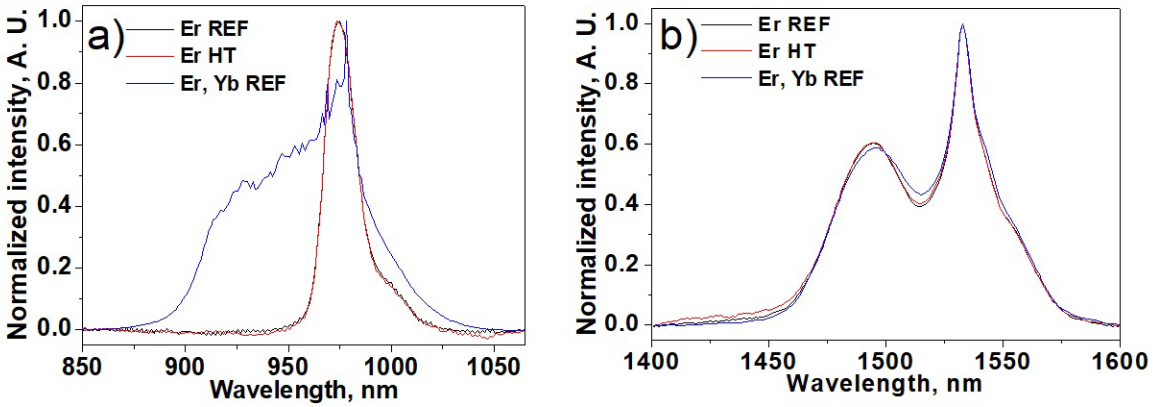

Figure 41. Comparison of absorption spectra of the fibers at: a) 980 nm; b) 1.5 µm.

The absorption spectra of the fibers were inversed and normalized to allow one to compare the shape of the band. Er REF and Er HT fibers exhibit similar absorption bands at 980 nm and 1.5 µm indicating that the Er^{3+} ions have similar site in both fibers and so that the heat treatment has no impact on the Er^{3+} site. Shape of the absorption spectra of the Er, Yb REF fiber was found the same as in [Gu, 17].

The emission spectra of the fibers were measured using an excitation at 972 nm and are shown in fig. 42. As explained in [Gu, 17], the length of the fibers has an impact on the shape of the emission band. Therefore, the emission spectra of fibers with different lengths were measured.

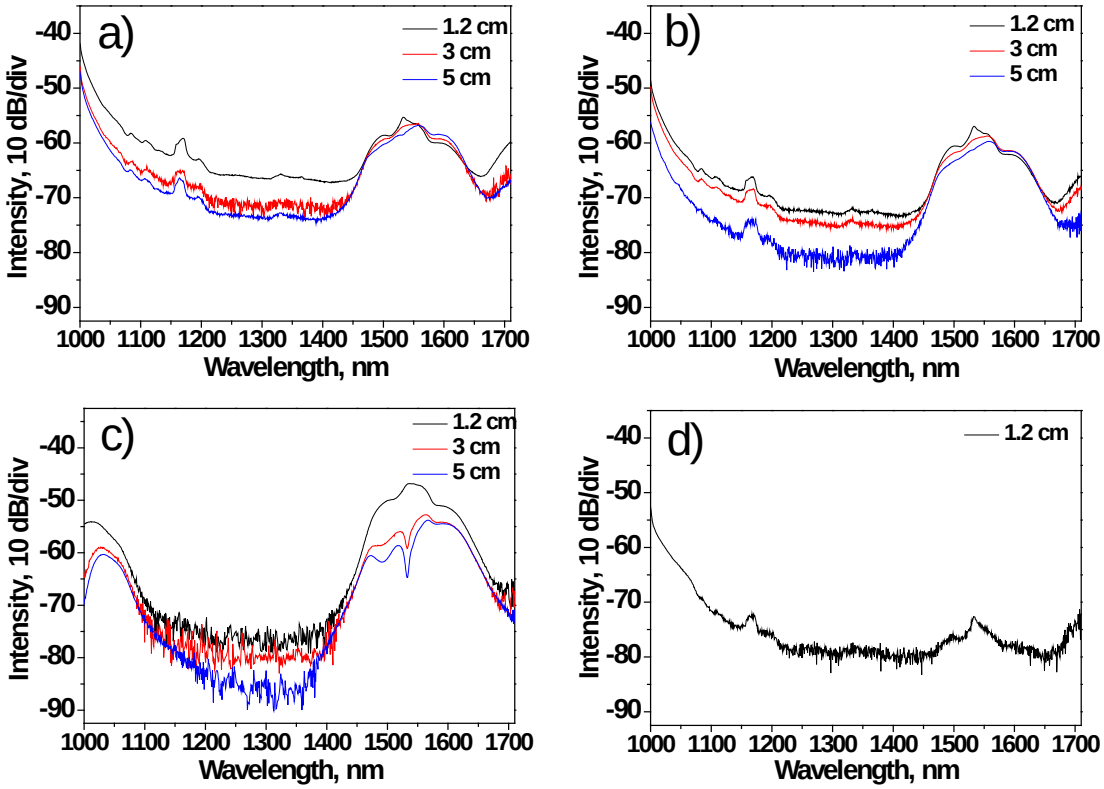

Figure 42. Emission spectra as a function of length: a) Er REF fiber; b) Er HT fiber; c) Er, Yb REF fiber; d) Er, Yb NPs fiber (1.2 cm long).

The fibers with short length exhibit an emission band, the shape of which is typical of the transition from $^4I_{13/2}$ to $^4I_{15/2}$ state of Er^{3+} ions in glass matrix. As seen in [Gu, 17], the shape of the emission band depends on the fiber length, especially for the Er, Yb REF fiber; it exhibits pronounced peaks and dips which are a clear sign of spectral hole burning effect [Na, 08]. These changes are due to reabsorption of the peak wavelength at 974 nm by Yb^{3+} ions and at 1534 nm by Er^{3+} ions originated from high concentration of the rare-earth ions and insufficient pump level to stimulate luminescence as explained in [Gu, 17].

One should point out that for the Er, Yb NPs fiber it was not possible to detect emission from 5 or 3 cm long fibers because of the low output. It is the bad quality of the fiber, the inhomogeneous distribution of the nanocrystals in the glass and their degradation in the glass during the melting, which are thought to lead to fiber with low emission. Nonetheless, the emission band from this fiber is broad indicating that the Er^{3+} ions are most probably located in an amorphous site in agreement with the analysis of the absorption spectra of the fiber.

One can notice an emission with small intensity in the 1150-1210 nm region in the spectra of the Er REF, Er HT and Er, Yb NPs fibers. This emission could be caused by transition between $^4F_{9/2}$ and $^4I_{13/2}$ states of Yb^{3+}.

The normalized emission band of 1.2 cm long fibers is shown in fig. 43.

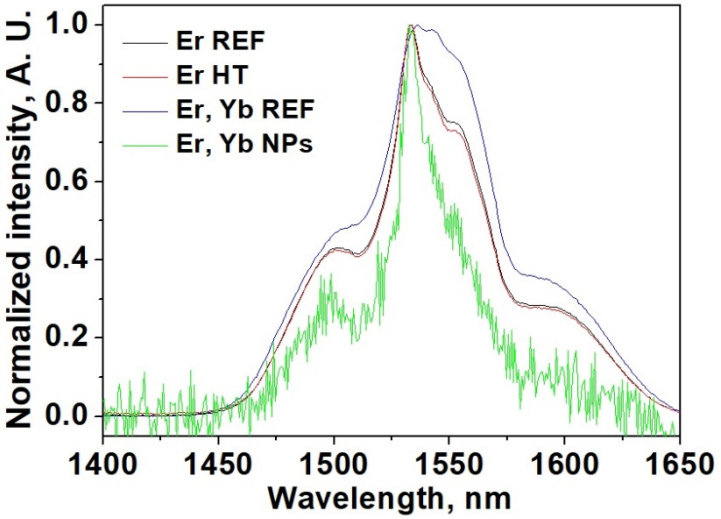

Figure 43. Normalized emission band for 1.2 cm long investigated fibers.

It is clearly shown that the composition of the glass has an impact on the shape of the emission band and so on the site of Er^{3+} ions. The heat treatment of the Er REF fiber has not impact on the shape of the emission indicating that if Ag nanoparticles are within the glass after heat treatment, they do not have an impact on the site of the Er^{3+} ions.

The emission band of Er^{3+} in the Er, Yb NPs fiber is less broad compared to the other fibers. Additionally, it exhibit a peak at ~1500 nm which might indicate that this emission band is from Er^{3+} ions in amorphous site but also from Er^{3+} located in $NaYF_4$: Er^{3+}, Yb^{3+}. Indeed, as shown in fig 44, the emission band of $NaYF_4$: Er^{3+}, Yb^{3+} exhibits peaks, one of them being at 1500 nm.

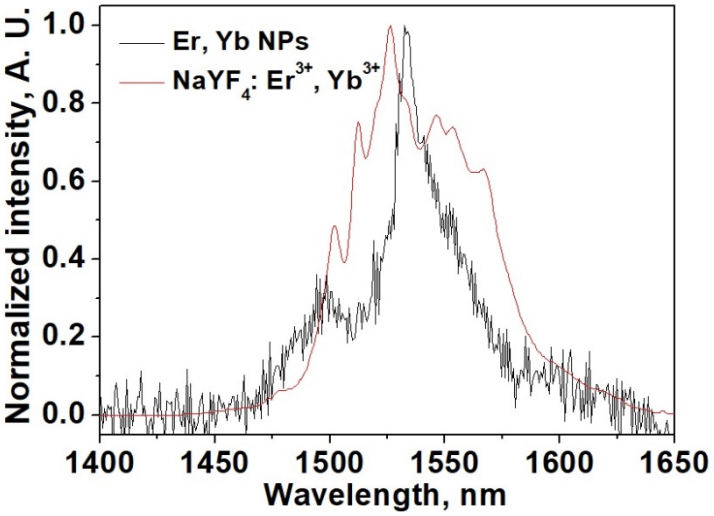

Figure 44. Normalized emission band for 1.2 cm long Er, Yb NPs fiber and $NaYF_4$: Er^{3+}, Yb^{3+} nanoparticles.

The upconversion spectra of the Er^{3+}, Yb^{3+}-codoped fibers were measured using an excitation at 972 nm but upconversion could not be detected in the Er, Yb NPs fibers. The upconversion spectrum of the Er, Yb REF fiber is presented in fig. 45.

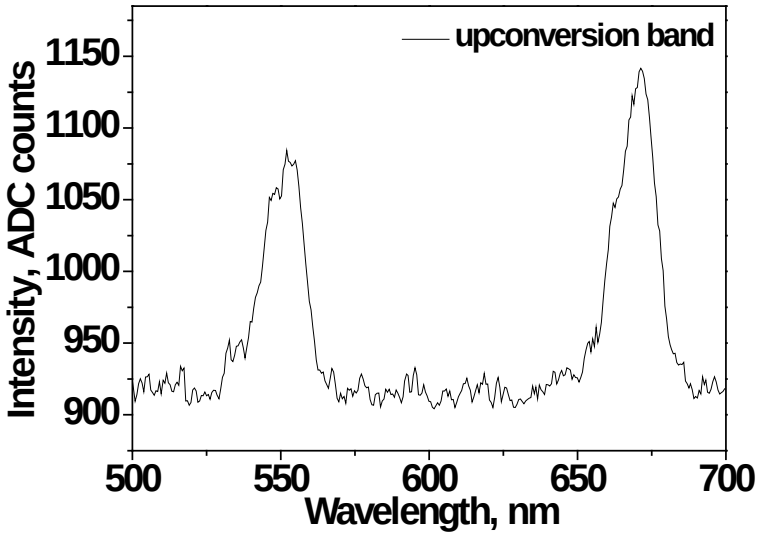

Figure 45. Upconversion spectrum of the Er, Yb REF fiber. Spectrum was obtained using laser diode source with excitation 972 nm.

The upconversion emission spectrum exhibits two bands at 550 and 670 nm, which are due to the transition $^2H_{11/2}$-$^4I_{15/2}$ and $^4S_{3/2}$-$^4I_{15/2}$ for green emission and $^4F_{9/2}$-$^4I_{15/2}$ for red emission [Oj, 18].

4.2 Testing the sensing properties of the fiber

The testing work was focused on the Er, Yb REF fiber as this fiber had better quality than the other fibers.

The sensing properties of the fibers were tested by measuring the emission spectra of the fibers in contact with N-Methylaniline (NMA), which is known to have an absorption band at 1500 nm (see fig. 46).

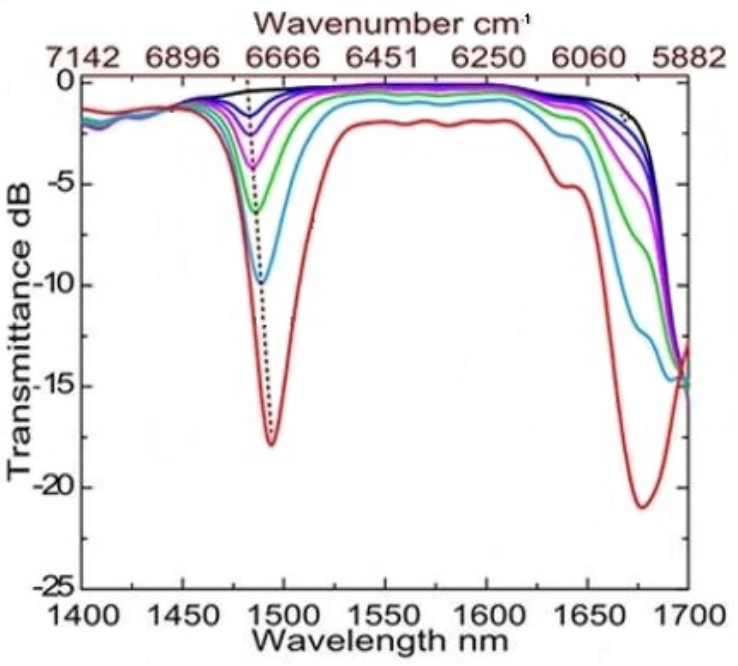

Figure 46. Absorption spectrum of the N-Methylaniline (NMA) solutions with hexane [Ka, 16]. Black curve shows pure hexane spectrum, other curves correspond to NMA diluted in hexane in different proportions (blue 4.2 vol%, purple 8.28 vol%, pink 16.57 vol%, green 33.3 vol%, light-blue 66.67 vol%) and red curve shows spectrum of the pure NMA.

At first, 5 cm fibers were immersed in 2 ml of different solutions containing N-Methylaniline (NMA). Two solutions were tested: a pure solution of NMA and a solution containing 20 volume % of NMA in ethanol. The normalized emission spectra are shown in fig. 47.

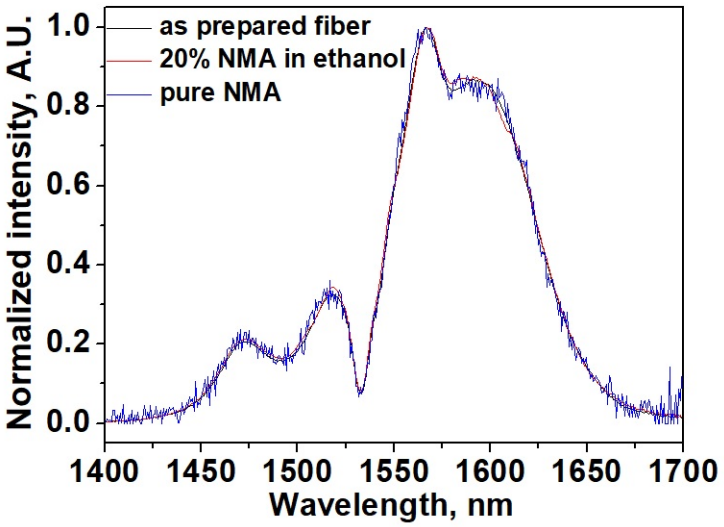

Figure 47. Normalized emission spectra of 5 cm long Er, Yb REF fiber in contact with the solution containing 20 volume % of N-Methylaniline (NMA) in ethanol and in pure NMA.

No changes in the shape of the emission band were observed when in contact with N-Methylaniline. Because of the reabsorption occurring in 5 cm long Er, Yb REF fibers, 1.5 cm long fibers were tested. As the fibers were too short for the mold, the fibers were placed on a holder and drops of the solution were deposited at the surface of the fibers.

A solution of 50% volume of NMA in ethanol and pure NMA were used in this experiment. The normalized emission spectra are shown in fig. 48a and b, respectively.

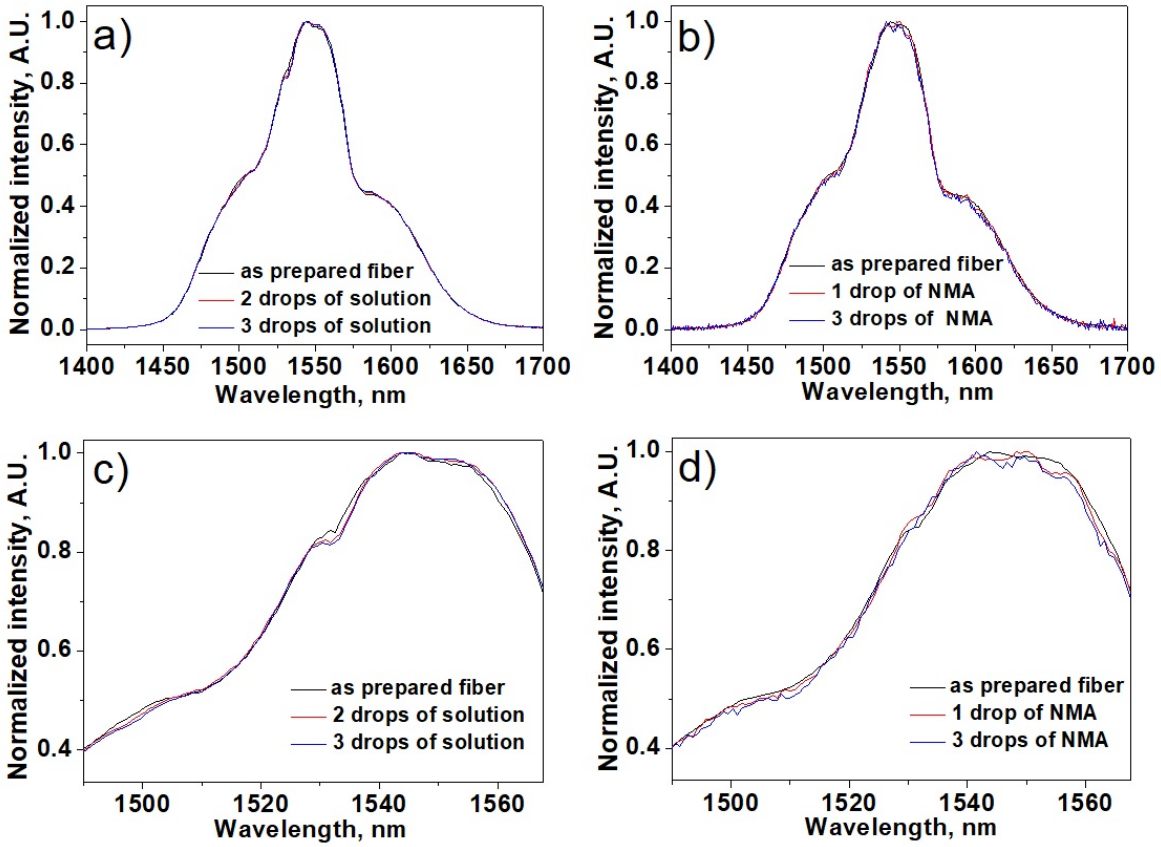

Figure 48. Normalized emission spectra of 1.5 cm long Er, Yb REF fiber: a) in contact with a solution 50 volume % of N-Methylaniline (NMA) in ethanol; b) in contact with pure NMA; c) zoom of the spectra sown in a; d) zoom for the spectra shown in b.

When in contact with NMA, it is possible to see that the intensity of the shoulder at 1500 nm decreases very slightly as shown in fig 47c and d. Some changes in the 1540 and 1560 nm region can be seen in fig. 47d, but they cannot be related to the absorption of NMA. From our experiment, it is not clear if the experimental setup can be used to test the sensing properties of the fiber when in contact with NMA.

5 CONCLUSION

New Er^{3+} doped and Er^{3+}, Yb^{3+}-codoped phosphate fibers (with the composition $82.8NaPO_3$-$9.2NaF$-$5ZnO$-$2.5Ag_2O$-$0.5Er_2O_3$, $49P_2O_5$-$39.2SrO$-$9.8Na_2O$-$0.5Er_2O_3$-$1.5Yb_2O_3$, and addition of $NaYF_4$: Er^{3+}, Yb^{3+} nanoparticles in $83.25NaPO_3$-$9.25NaF$-$5ZnO$-$2.5Ag_2O$) were investigated in this study.

During this study, the fiber drawing process was found to lead to some changes in the thermal properties of the glasses leading to a significant decrease in ΔT, which is a gauge of the thermal stability of the glass against crystallization. Within the accuracy of the EDS measurement, the compositions of the investigated fibers were found to be the same than the corresponding preforms, confirming that the drawing process was under control and did not lead to significant evaporation of the glass components. Using SEM, the surface of the fibers were found to be damaged, most probably due to aging. These damages could be due to water absorption as the glasses are known to be hygroscopic. Although the fibers have bad surface quality, the absorption and emission spectra were successfully measured. Typical absorption and emission bands of $Er^{3+}$and Yb^{3+} were detected. Based on the shape of the emission band, some $NaYF_4$: Er^{3+}, Yb^{3+} nanoparticles are suspected to remain in the fiber although no upconversion could be detected from this fiber. Emission measurements were performed from fibers with different lengths (1.2, 3 and 5 cm) and reabsorption was observed in fiber which contains large amount of $Er^{3+}$and Yb^{3+}. However, we found that this fiber exhibits upconversion.

While testing sensing properties of the Er, Er REF fibers, small changes in the shape of the emission band were observed when in contact of N-Methylaniline but it is still unclear if the experimental setup can be used to study the sensing properties of fibers. This needs further investigation.

This research was done to check that the drawing process has no significant impact on the thermal, structural and optical properties of the fibers and check if it is possible to use them for sensing in future applications. To continue this research, new fibers with a polymer jacket should be drawn to slow down the aging of the fibers and to limit water absorption.

6 REFERENCES

[Ab, 09] E. A. Abou Neel, W. Chrzanowski, D. M. Pickup, L. A. O'Dell, N. J. Mordan, R. J. Newprot, M. E. Smith, J.C. Knowles. "Structure and properties of strontium-doped phosphate-based glasses", J. R. Soc. Interface 6, pp. 435-446, 2009

[Ac, 12] D. E. Achatz. "Synthesis and Surface Modification of Luminescent Nanoparticles for Imaging and Sensing of Oxygen Using Near-Infrared Excitation", pp. 7-8, 2012

[Al] A. Al-Yasiri. "Production and Characteristics of X-Rays", https://www.slideshare.net/AmalAlYasiri/production-and-characteristics-of-xrays [Retrieved 16.05.2019]

[Ba, 06] Rolindes Balda. "Photonic glasses", Research Signpost, pp. 24-115, 2006.

[Br, 00a] R. K. Brow. "Review: the structure of simple phosphate glasses", J. Non-Cryst. Solids 263&264, Elsevier, pp. 2-11, 2000

[Br, 00b] R. K. Brow, C. A. Click, T. M. Alam. "Modifier coordination and phosphate glass networks", J. Non-Cryst. Solids 274, Elsevier, pp. 9-16, 2000

[Br, 94] S. Bruni, F. Cariati, D. Narducci. "Infrared specular reflection spectra of copper-zinc phosphate glasses", Vib. Spectrosc. 7, pp. 169-173, 1994

[Bu, 09] M. M. Bubnov, V. N. Vechkanov, A. N. Gur'yanov, K. V. Zotov, D. S. Lipatov, M. E. Likhachev, M. V. Yashkov. "Fabrication and optical properties of fibers with an Al_2O_3-P_2O_5-SiO_2 glass core", Inorg. Mater. 45, pp. 444-449, 2009

[Bu, 10] G. W. Burdick, J. B. Gruber, K. L. Nash, S. Chandra, D. K. Sardar. "Analyses of $4F^{11}$ Energy Levels and Transition Intensities Between Stark Levels of Er^{3+} in $Y_3Al_5O_{12}$", Spectroscopy Letters 34, pp. 406-422, 2010

[Bu, 14] B. Bureau, C. Boussard, S. Cui, R. Chahal, M. L.Anne, V. Nazabal, O. Sire, O. Loreal, P. Lucas, V. Monbet, J.-L. Doualan, P. Camy, H. Tariel, F. Charpentier, L. Quentel, J.-L. Adam, J. Lucas. “Chalcogenide optical fiber for mid-infrared sensing”, Optical Engineering 53 (2) 027101, pp. 1-7, 2014

[Cu, 13] S. Cui, R. Chahal, C. Boussard-Pledel, V. Nazabal, J.-L. Doualan, J. Troles, J. Lucas, B. Bureau. “From Selenium- to Tellurium-Based Glass Optical Fibers for Infrared Spectroscopies”, Molecules 18 (5), pp. 5373-5388, 2013

[Du, 03] A. Duncan. “The Technique of Leaded Glass”, Dover Publications, Inc., pp. 31, 2003

[Dy] A. Dybko. Chemical Sensors Research Group, http://csrg.ch.pw.edu.pl/tutorials/fiber/ [Retrieved 16.05.2019]

[En, 06] “Erbium (revised).” Chemical Elements: From Carbon to Krypton, 2006. https://www.encyclopedia.com/science/news-wires-white-papers-and-books/erbium-revised [Retrieved 30.04.2019]

[Ga, 04a] H. Gao, T. Tan, D. Wang. “Effect of composition on the release kinetics of phosphate controlled release glasses in aqueous medium”, J. Control. Release 96, pp. 21-28, 2004

[Ga, 04b] P. Gangodpanhyay, P. Magudapathy, R. Kesavamoorthy, B. K. Panigrahi, K. G. M. Nair, P. V. Satyam. “Growth of silver nanoclusters embedded in soda glass matrix”, Chem. Phys. Lett., 388: 416, 2004

[Gl] https://www.gla.ac.uk/schools/ges/researchandimpact/researchfacilities/isaac/services/scanningelectronmicroscopy/ [Retrieved 16.05.2019]

[Gu, 17] R. Gumenyuk, A. Poudel, T. Jouan, C. Boussard-Pledel, T. Niemi, L. Petit. “Super-luminescence and spectral hole burning effect in ultra-short length Er/Yb-doped phosphate fiber”, Optical material express 7 (12), pp. 4358-4366, 2017

[Hu, 01] Y. Hu, S. Jiang, T. Luo, K. Seneschal, M. Morell, F. Smektala, S. Honkanen, J. Lucas, N. Peyghambarian. “Performance of high-concentration Er^{3+} - Yb^{3+} -codoped phosphate fiber amplifiers”, IEEE Photonics Technol. Lett. 13 (7), pp. 657-659, 2001

[Il, 01] D. Ilieva, B. Jivov, D. Kovacheva, T. Tsacheva, Y. Dimitriev, G. Bogachev, C. Petkov. “FT-IR and Raman spectra of Gd phosphate crystals and glasses”, J. Non-Cryst. Solids 293, pp. 562–568, 2001

[In, 16] B. J. Inkson. “Scanning electron microscopy (SEM) and transmission electron microscopy (TEM) for materials characterization”, Materials Characterization Using Nondestructive Evaluation (NDE) Methods, Elsevier pp. 17-43, 2016

[In, 19] Interwire, 2019, https://www.wireweb.de/wire-reports/measuring-solutions-for-fibre-optic%C2%A0manufacturing-processes_35749_de/ [Retrieved 16.05.2019]

[Ji, 00] S. Jiang, T. Luo, B.C. Hwang, F. Smekatala, K. Seneschal, J. Lucas, N. Peyghambarian. “Er^{3+}-doped phosphate glasses for fiber amplifiers with high gain per unit length”, J. Non-Cryst. Solids 263, pp. 364-368, 2000

[Ji, 16] C. Jiang, X. Wang, M. Zhu, H. Xu, Q. Nie, S. Dai, G. Tao, X. Shen, C. Cheng, Q. Zhu, F. Liao, P. Zhang, P. Zhang, Z. Liu, X.-H. Zhang. “Preparation of chalcogenide glass fiber using an improved extrusion method”, Optical Engineering 55 (5) 056114, pp. 1-8, 2016

[Ka, 99] S. O. Kasap. “Optoelectronics”, Prentica Hall, 1999

[Ka, 09] S. O. Kasap, H. Ruda, Y. Boucher. “Cambridge illustrated handbook of optoelectronics and photonics”, Cambridge University Press, 2009

[Ka, 16] A. Karabchevsky, A. V. Kavokin. “Giant absorption of light by molecular vibrations on a chip”, Sci. Rep. 6 (21201), 2016

[Kn, 03] J. C. Knowles, “Phosphate based glasses for biomedical applications”, J. Matter. Chem. 13, pp. 2395-2401, 2003

[Ko, 10] I. Konidakis, C. P. E. Varsamis, E. I. Kamitsos, D. Möncke, D. Ehrt. “Structure and properties of mixed strontium-manganese metaphosphate glasses”, J. Phys. Chem. 114, pp. 9125-9138, 2010

[La, 15] T. Laihinen, M. Lastusaari, L. Pihlgren, L. C. V. Rodrigues, J. Hölsä. J. Therm. Anal. Calorim. 121, pp. 37-43, 2015

[Le] https://www.lemerpax.com/en/products/radiation-shielding-windows/ [Retrieved 16.05.2019]

[Le, 13] P. Le Parlouer. “Thermal Analysis and Calorimetry Techniques for Catalytic Investigations”, Calorimetry and Thermal Methods in Catalysis, Springer, pp. 51-101, 2013

[Lu, 99] X. Lu, E. M. Arruda, W. W. Schultz. “The effect of processing parameters on glass fiber birefringence development and relaxation”, J. Non-Newtonian Fluid Mech. 86, pp. 89-104, 1999

[Ma, 09] J. Massera. “Nucleation and growth behaviour of tellurite-based glasses suitable for mid-infrared applications”, PhD dissertation, Graduate school of Clemson University, 2009

[Me, 97] K. Meyer. “Characterization of the structure of binary zinc ultraphosphate glasses by infrared and Raman spectroscopy”, J. Non-Cryst. Solids 283, pp. 227-239, 1997

[Mi, 13] C. Ming, F. Song, H. Liu. J. Non-Cryst. Solids 360, pp. 1-3, 2013

[Mo, 98] Y. M. Moustafa, K. El-Egili. “Infrared spectra of sodium phosphate glasses”, J. Non-Cryst. Solids 240, pp. 144-153, 1998

[Na, 08] P. Nandi, G. Jose. “Superfluorescence from Yb- and Yb-Er-doped phosphotellurite glass fibers”, Opt. Fiber Technol. 14 (4), pp. 275-280, 2008

[Nd] NDT Resource Center, Center for NDE, Iowa State University, https://www.nde-ed.org/EducationResources/CommunityCollege/Materials/Structure/solidstate.php [Retrieved 16.05.2019]

[Oj, 18] N. Ojha, M. Tuomisto, M. Lastusaari, L. Petit. “Upconversion from fluorophosphate glasses prepared with NaYF4: Er^{3+}, Yb^{3+} nanocrystals”, RSC Advances J. 8 (34), pp. 19226-19236, 2018

[Om, 99] M. A. Omary, H. H. Patterson. “Luminescence Theory”, Encyclopedia of Spectroscopy and Spectrometry, Elsevier, pp. 1372-1391, 1999

[Os] Osioptics, https://www.osihardware.com/wp-content/uploads/2018/08/osi-optics-smartoptics-optical-fibers.pdf [Retrieved 16.05.2019]

[Pe, 16] A. Perro, G. Lebourdon, S. Henry, S. Lecomte, L. Servant, S. Marre. “Combining microfluidics and FT-IR spectroscopy: towards spatially resolved information on chemical processes”, React. Chem. Eng. 1, pp. 557-594, 2016

[Pe, 17a] O. PeŠek, J. Melcher. “Shape and size of initial geometrical imperfections of structural glass members”, Civil Engineering Series 17 (1), p. 160, 2017

[Pe, 17b] S. P. Peddi, H. Mathlouthi, B. A. Sadeh, M. A. Yehdih. “Up and Downconversion Luminiscence Studies of Erbium Doped Yttrium Oxide Nanoparticles for Sensing Applications”, AUSEJ 2, pp. 23-27, 2017

[Po, 17] A. Poudel, I. Dmitrieva, R. Gumenyuk, L. Mihai, D. Sporea, O. Muresan, I. Rusen, T. Hakkarainen, N. G. Boetti, T. Niemi, L. Petit. “Effect of ZnO Addition and of Alpha Particle Irradiation on Various Properties of Er^{3+}, Yb^{3+} Doped Phosphate Glasses”, Applied Science 7, p. 1094, 2017

[Pr, 04] P. N. Prasad. “Nanophotonics”, Wiley, 2004

[Qu, 06] Richard S. Quimby. “Photonics and Lasers: An Introduction”, John Wiley & Sons, pp. 1, 2006

[Se, 09] J. M. Senior, M. Y. Jamro. “Optical fiber communications: principles and practice”, Financial Times/Prentice Hall, 2009

[Se, 16] https://sellbroke.com/2016/06/10/everything-need-know-recycling-rare-earth-elements/ [Retrieved 16.05.2019]

[Sh, 05] J. E. Shelby. “Introduction to Glass Science and Technology”, 2nd edition, 2005

[Sh, 07a] H. Shalibeik, “Rare-earth-doped Fiber Lasers and Amplifiers”, Cuvillier Verlag, 2007

[Sh, 07b] P. Y. Shih, H. M. Shiu. “Properties and structural investigations of UV-transmitting vitreous strontium zinc metaphosphate”, Mater. Chem. Phys. 106, pp. 222-226, 2007

[St, 07] C. Strumpel. “Modifying the solar spectrum to enhance silicon solar cell efficiency – an overview of available materials”, Solar Energy Materials and Solar Cells 91 (4), pp. 238-249, 2007

[St, 16] C. Stanley, A. Mojiri, G. Rosengarten. “Spectral light management for solar energy conversion systems”, Nanophotonics 5 (1), De Gruyter Open, pp. 161-179, 2016

[Tb, 17] Tech Briefs. “High-Power Fiber Lasers”, p. 1, https://www.techbriefs.com/component/content/article/23-ntb/features/feature-articles/26467-high-power-fiber-lasers?Itemid=114 [Retrivied 16.05.2019]

[Th] Tobias A. Thiele. “DURAN Group celebrates 120 years of laboratory glassware made from borosilicate glass”, https://www.bionity.com/en/whitepapers/126361/duran-group-celebrates-120-years-of-laboratory-glassware-made-from-borosilicate-glass.html [Retrivied 30.04.2019]

[Th, 07] K. Thyagarajan, A. Ghatak. “Fiber Optic Essentials”, Elsevier, 2007

[Ti, 14] L. Tian, Z. Xu, S. Zhao, Y. Cui, Z. Liang, J. Zhang, and X. Xu. “The upconversion luminescence of $Er^{3+}/Yb^{3+}/Nd^{3+}$ triply-doped β-$NaYF_4$ nanocrystals under 808-nm excitation”, Materials 7 (11), pp. 7289-7303, 2014

[Vo, 94] Werner Vogel. “Glass chemistry”, 2nd edition, Springer-Verlag Berlin Heidelberg, 1994

[Wi, 05] https://commons.wikimedia.org/wiki/File:Electron_shell_068_erbium.png [Retrieved 16.05.2019]

[Wi, 11] https://commons.wikimedia.org/wiki/File:FTIR_Interferometer.png [Retrieved 16.05.2019]

[Wi, 84] J. A. Wilder, J. E. Shelby. “Property variation in alkali alkaline-earth metaphosphate glasses”, J. Am. Ceram. Soc. 67, pp. 438-444, 1984

[Ya, 00] M. Yamane, Y. Asahara. “Glasses for Photonics”, Cambridge University Press, 2000

[Ye, 12] Chai Yeh. “Applied Photonics”, Elsevier, pp. 1-6, 2012

[Yu, 13] S. W. Yung, Y. S. Huang, Yi-Mu Lee, Y. S. Lai. “An NMR and Raman spectroscopy study of Li_2O-SrO-Nb_2O_5-P_2O_5 glasses”, RSC Advances J. 43, 2013

[Yu, 16] Y. Yao, C. Xu, Y. Zheng, C. Yang, P. Liu, T. Jia, J. Qiu, Z. Sun, S. Zhang. “Femtosecond Laser-Induced Upconversion Luminescence in Rare-Earth Ions by Nonresonant Multiphoton Absorption”, J. of Phys. Chem. A 120, pp. 5522-5526, 2016